ELECTRONIC SUPPORTING INFORMATION

Key structural features to favour imines over hydrates in water: pyridoxal phosphate as a muse

Ferran Esteve,* Tanguy Rieu, Jean-Marie Lehn*

Laboratoire de Chimie Supramoléculaire, Institut de Science et d'Ingénierie Supramoléculaires (ISIS), Université de Strasbourg, 8 allée Gaspard Monge, 67000 Strasbourg, France

Table of contents

1. Experimental section

1.1. Materials and methods

All amines, aldehydes **A0-A10** and components of buffer solutions were obtained from commercial suppliers and used without further purification. Glutamic-Pyruvic Transaminase (**GPT**) was obtained from Sigma-Aldrich and used without further treatment since this enzyme already contained **PLP** as a cofactor. A Mettler Toledo SevenCompact pH Meter S220 was used to monitor the pD of the solutions, adjusted with either NaOD or DCl solutions as appropriate. All reactions were performed at room temperature, unless otherwise noted. Imination reactions were carried out in 50 mM deuterated phosphate buffer pD 7.0 unless otherwise indicated. The yields and product abundances were determined by relative integration of the signals in the 500 MHz ^{1}H-NMR spectra (Bruker Ascend Spectroscope Advance Neo-500 MHz; 500 MHz for ^{1}H and 126 MHz for $^{13}C\{^{1}H\}$). First, the spectrum was referenced, phased, and the baseline was corrected. Afterwards, the signals of interest were accurately integrated to minimise the residual error, and finally, the numerical values are for calculating product abundances. The error in integration is of 5%. An example of the procedure is illustrated in Fig. S19. All the reactions were analysed after 10 min, 1 h, 24 h, and 48 h to confirm that the equilibrium state was reached. The equilibrium was attained in all reactions after 10 min, except for the condensations between **B1** and **A12** / **A13** / **A14** in which *ca.* 3 h were needed. Data analysis was performed using MestReNova (version 14.2.3) and OriginPro (version 9.8.0.200). HRMS-electro-spray ionization (HRMS-ESI) mass spectra were recorded using a ThermoFisher Exactive Plus EMR Orbitrap mass spectrometer. FTIR (ATR) were measured using a Thermofischer FTIR iS50. See Fig. S20-S35 for characterization.

1.2. DFT calculations

DFT calculations were performed at the b3lyp level of theory using the 6-31g(d,p) basis set.[1] The DFT models were calculated at room temperature and using water as the solvent (PCM).[2] All free energies (kcal/mol) were calculated taking into account the energies of the corresponding reagents and the molecule of water released in the condensation reaction. All stationary points were characterized at this level of theory by analytical frequency calculations as minima (all positive eigenvalues). In addition, single-point dispersion corrections were computed using Grimme's D3 parameter set and zero damping.[3] 3D representations were designed using the CylView software. The electron density surfaces (EDS) of the *chk*. file were represented using Jmol software with the isosurface density values ranging from -0.7 to 0.5 a.u, using the "RGB" style. NBO analysis was implemented by NBO 3.1 module in Gaussian 09 packages and presented using Jmol. See "DFT details" section for energies and Cartesian coordinates of the different species.

1.3. Buried volume calculation using SambVca

The buried volumes and steric maps were calculated using the SambVca web server,[4,5] under the GNU general public license.[6] The input files (.xyz) were built by choosing the most stable conformation calculated for each of the aldehydes (*viz.* **A0**, **PLP**, **A10**, **A11**, **A12**, **A13**, **A14** and **A15**) using DFT (see DFT section). To generate the steric map, the aldehyde structure was oriented in a Cartesian frame with a selected point at the origin, corresponding to the centre of the sphere that will dictate the volume of interest (in our case the origin was the C atom of the carbonyl group, C1 in Fig. S36). Then, a second atom was selected to determine the direction of the z-axis (C2 in Fig. S36), and a third point to establish the xz-plane (consisting of two atoms C3 and C7, Fig. S36). After alignment of the molecule, we removed the atoms that must be excluded from the steric map calculations. In this project, since the objective was to evaluate the crowding effect of the *ortho*-substituents around the carbonyl unit, all atoms except the ones pertaining to the substituents were removed (*e.g.,* atoms: O1, H1, C1, C2, C3, C4, H2, C5, H3, C6, H4, C7 in Fig. S36). Thereafter, a sphere of radius 4.5 Å, centred at the origin, was sectioned by a regular three-dimensional cubic mesh of spacing 0.1, which defines the cubic voxels. The distance between the centre of each voxel with all the atoms of the aldehyde was studied to evaluate if any of the atoms were within the van der Waals distance from the centre of the examined voxel. If no atom was within the van der Waals distance, the examined voxel was marked as a free voxel, and otherwise the examined voxel was marked as buried. Then, the program scans the sphere and provides a surface indicating the free and buried volumes (%). For the atoms, we adopted the option “bondi radii scaled by 1.17”, and the hydrogen atoms were **,** considered to build the steric maps (because they are important for **A0**, **PLP**, **A10**, **A11** and **A15**). The resulting maps are simple two-dimensional isocontour representations of the interaction surfaces. See Fig. S37-S44 for maps and buried and free volume (%) data.

1.4. Synthetic protocols

The general protocol was adapted from reference 7 (reference 29 in main text).

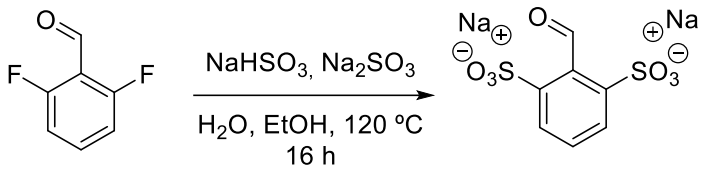

A12

Synthesis of A12. 2,6-difulurobenzaldehyde (1 eq., 0.55 g, 3.84 mmol) was dissolved in EtOH (5 ml) in a 50 mL round-bottom flask. $NaHSO_3$ (0.3 eq., 0.12 g, 1.15 mmol) and Na_2SO_3 (3 eq., 1.45 g, 11.53 mmol) were then poured into the solution of the aldehyde, and H_2O (5 mL) was introduced under vigorous stirring. The resultant suspension was refluxed at 120 ºC for 16 h. The mixture was then cooled down to room temperature and it was poured into 50 mL of MeOH, observing the formation of abundant white precipitate. This precipitate was filtered-off and the resultant solution was dried under reduced pressure. The white solid obtained was washed with boiling MeOH (3x5 mL) and dried overnight at 50 ºC under reduced pressure to yield pure **A12** as a white solid (311 mg, 1.00 mmol, 26%). Characterization: FTIR (ATR): 3511 (bs), 3094, 1714, 1642, 1186, 1037. ^{1}H-NMR (500 MHz, D_2O) δ (ppm) 10.51 (s, 1H), 7.93 (dd, J = 7.9, 1.0 Hz, 2H), 7.63 (td, J = 8.0, 1.0 Hz, 1H). ^{13}C{^{1}H}-NMR (126 MHz, D_2O) δ (ppm) 197.2, 141.4, 133.7, 130.9, 129.8. HRMS-QTOF(-) calcd for $C_7H_5O_7S_2$: 264.9482, found 264.9481. See Fig. S20-S22 and S32.

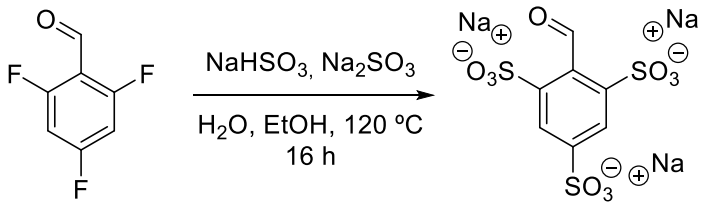

A13

Synthesis of A13. This compound was synthesized following the same procedure as described for **A12** but using 2,4,6-trifulurobenzaldehyde (1 eq., 0.72 g, 4.47 mmol), $NaHSO_3$ (0.5 eq., 0.24 g, 2.23 mmol) and Na_2SO_3 (5 eq., 2.81 g, 22.33 mmol). **A13** was obtained as a pure white solid after the 3 washes with boiling MeOH (0.62 g, 1.45 mmol, 32%). Characterization: FTIR (ATR): 3448 (bs), 3100, 1713, 1652, 1194, 1049. ^{1}H-NMR (500 MHz, D_2O) δ (ppm) 10.50 (s, 1H), 8.26 (s, 2H). ^{13}C{^{1}H}-NMR (126 MHz, D_2O) δ (ppm) 196.1, 144.8, 142.7, 136.1, 126.7. HRMS-QTOF(-) calcd for $C_7H_5O_{10}S_3$: 344.9050, found 344.9050. See Fig. S23-S25 and S33.

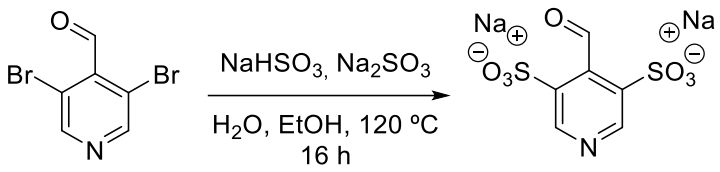

A14

Synthesis of A14. This compound was synthesized following the same procedure as described for **A12** but using 3,5-dibromopyridine-4-carbaldehyde (1 eq., 0.66 g, 2.49 mmol), $NaHSO_3$ (0.3 eq., 0.08 g, 0.75 mmol) and Na_2SO_3 (3 eq., 0.94 g, 7.47 mmol). **A14** was obtained as a pure white solid after the 3 washes with boiling MeOH (0.59 g, 1.88 mmol, 76%). Characterization: FTIR (ATR): 3607 (bs), 3405, 3094, 1713, 1640, 1201, 1038. ^{1}H-NMR (500 MHz, D_2O) δ (ppm) 10.49 (s, 1H), 9.05 (s, 2H). ^{13}C{^{1}H}-NMR (126 MHz, D_2O) δ (ppm) 194.8, 149.7, 141.9, 136.5. HRMS-QTOF(-) calcd for $C_6H_5O_7NS_2$: 265.9435, found 265.9434. See Fig. S26-S28 and S34.

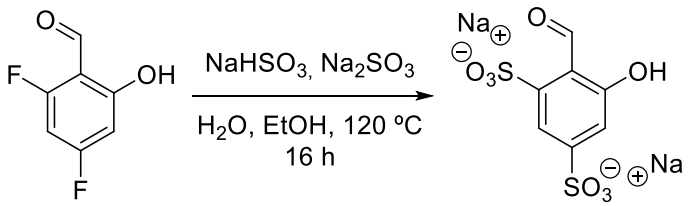

A15

Synthesis of A15. This compound was synthesized following the same procedure as described for **A12** but using 2,4-difluoro-6-hydroxybenzaldehyde (1 eq., 0.55 g, 3.48 mmol), $NaHSO_3$ (0.3 eq., 0.08 g, 1.05 mmol) and Na_2SO_3 (3 eq., 1.31 g, 10.44 mmol). **A15** was obtained as a pure yellow solid after reverse phase flash chromatography (C18, 100% H_2O as eluent) (0.22 g, 0.67 mmol, 19%). Characterization: FTIR (ATR): 3452 (bs), 3098, 1652, 1605, 1186, 1044. ^{1}H-NMR (500 MHz, D_2O) δ (ppm) 10.64 (s, 1H), 7.83 – 7.67 (m, 1H), 7.55 – 7.37 (m, 1H). ^{13}C{^{1}H}-NMR (126 MHz, D_2O) δ (ppm) 197.1, 162.2, 148.9, 146.1, 118.6, 116.8, 115.8. HRMS-QTOF(-) calcd for $C_7H_5O_8S_2$: 280.9431, found 280.9430. See Fig. S29-S31 and S35.

2. Main text supporting Figures and Tables

Table S1. Hammett parametres considered for the different substituents studied in this work:

Substituent	σ_m	σ_p [a]
-F [b]	0.34	0.06
$-NO_2$ [b]	0.71	0.78
-OH [b]	0.12	-0.37
$-O^-$ [b]	-0.47	-0.81
$-SO_3^-$ [b]	0.30	0.35
-Br [b]	0.39	0.23
$-CH_3$ [b]	-0.07	-0.17
2-N_{py} [c]	0.71	
3-N_{py} [c]	0.55	
4-N_{py} [c]	0.94	
2-N_{py}-H^+ [c]	3.11	
3-N_{py}-H^+ [c]	2.10	
4-N_{py}-H^+ [c]	2.57	

[a] The value of σ_p was also employed for *ortho*-substitution. [b] Values taken from reference 30 in main text.
[c] Values taken from reference 31 in main text.

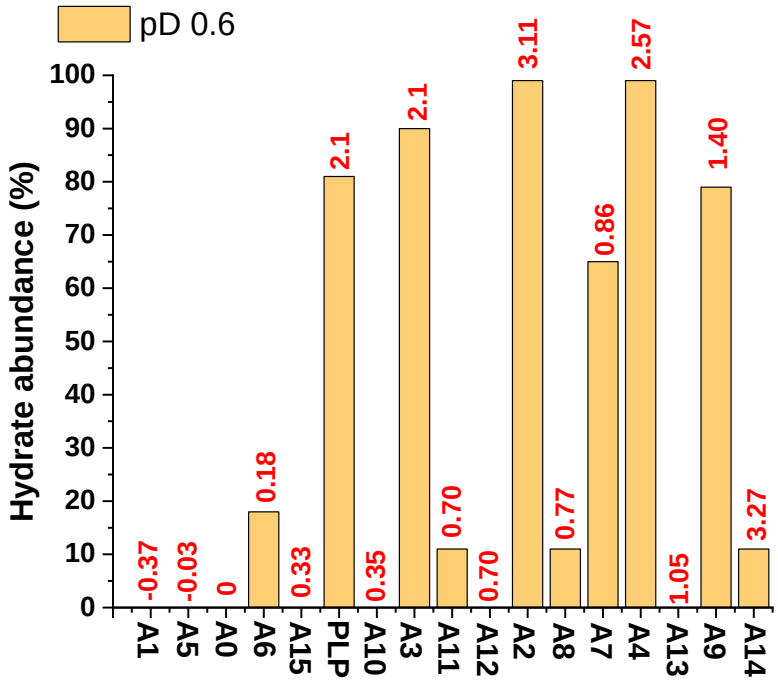

Fig. S1. Hydrate abundances (%) for the different aldehydes at pD 0.6. Red values correspond to the Hammett scores calculated at such pD. Reaction conditions: 5 mM aldehyde, D_2O, pD 0.6, 295 K, 1 h. Abundances determined by ^1H NMR spectroscopy (500 MHz, 295 K). Error in NMR measurements: 5%.

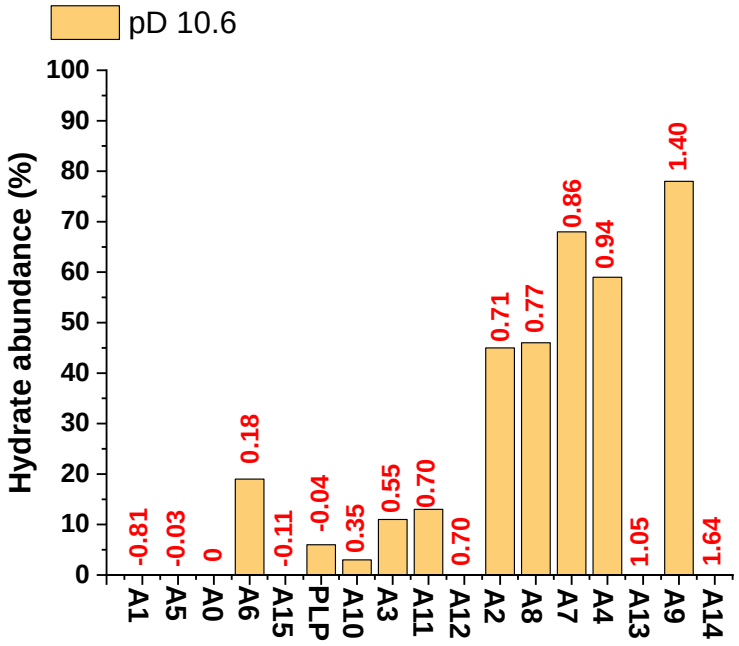

Fig. S2. Hydrate abundances (%) for the different aldehydes at pD 10.6. Red values correspond to the Hammett scores calculated at such pD. Reaction conditions: 5 mM aldehyde, D_2O, pD 10.6, 295 K, 1 h. Abundances determined by ^{1}H NMR spectroscopy (500 MHz, 295 K). Error in NMR measurements: 5%.

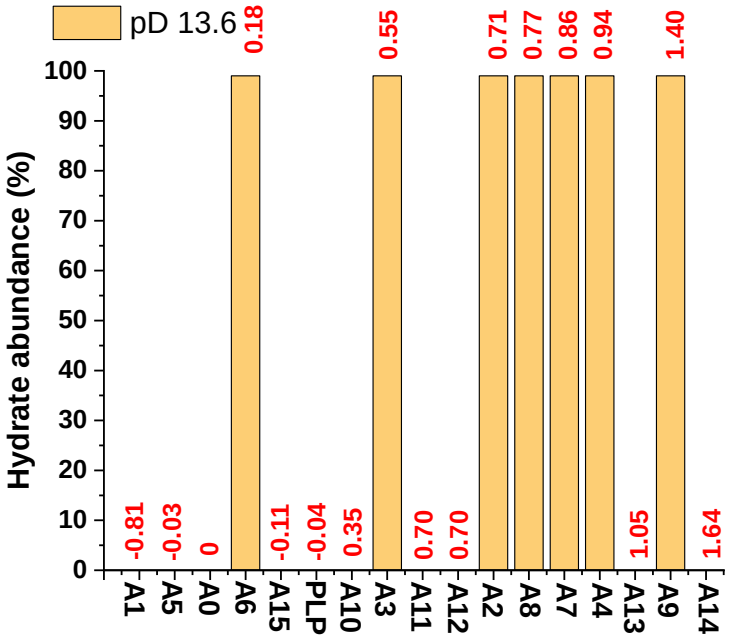

Fig. S3. Hydrate abundances (%) for the different aldehydes at pD 13.6. Red values correspond to the Hammett scores calculated at such pD. Reaction conditions: 5 mM aldehyde, D_2O, pD 13.6, 295 K, 1 h. Abundances determined by ^{1}H NMR spectroscopy (500 MHz, 295 K). Error in NMR measurements: 5%.

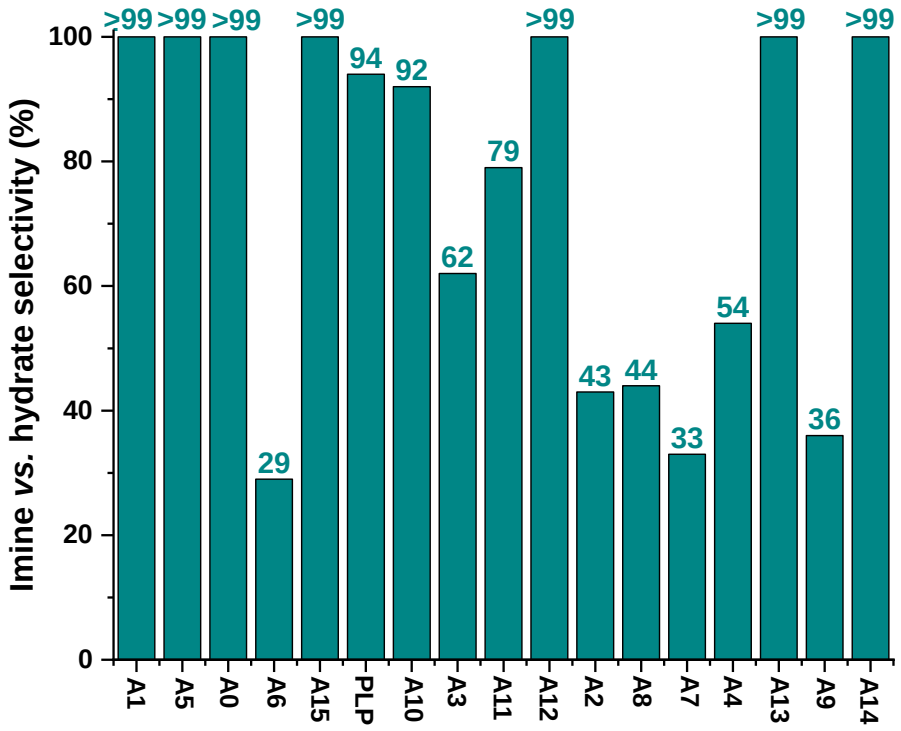

Fig. S4. Imine *vs.* hydrate selectivity calculated for the product distributions of Fig. 1E. The results have been sorted with increased ΣHammett values. See Table S1 for Hammett values used. Reaction conditions: 5 mM aldehyde and 5 mM **B1**, D_2O, pD 7.0 (50 mM PBS), 295 K, 3 h. Product abundances determined by ^1H NMR spectroscopy (500 MHz, 295 K). Error in measurements: 5%.

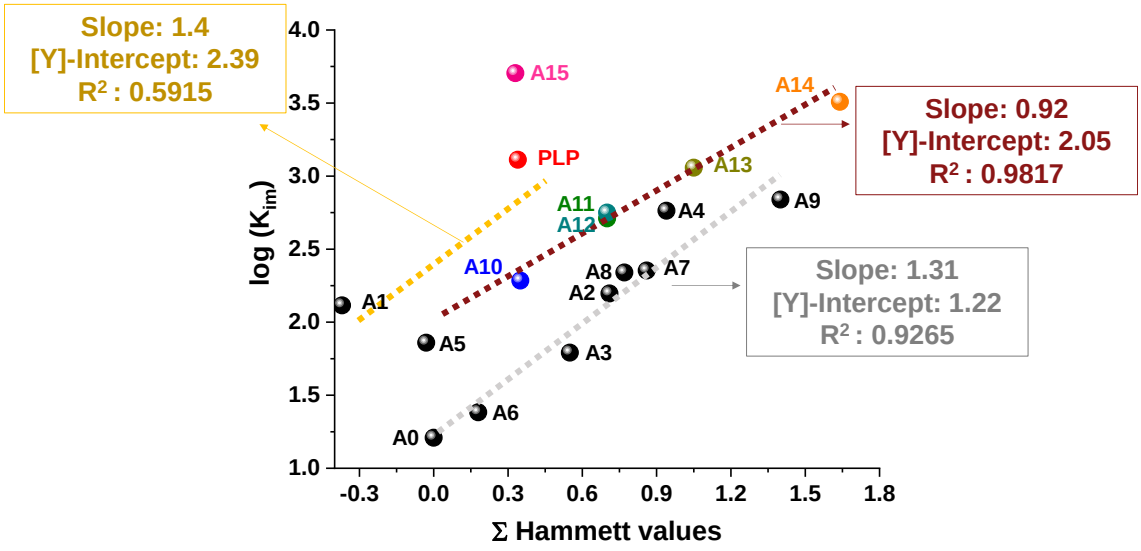

Fig. S5. Hammett plot of the log(K_{im}) for the addition of **B1** to the different aldehydes. The linear fittings (corresponding to the three families of compounds described in the main text) have been included. Reaction conditions: 5 mM aldehyde and 5 mM **B1**, D_2O, pD 7.0 (50 mM PBS), 295 K, 3 h. Error in measurements: 5%.

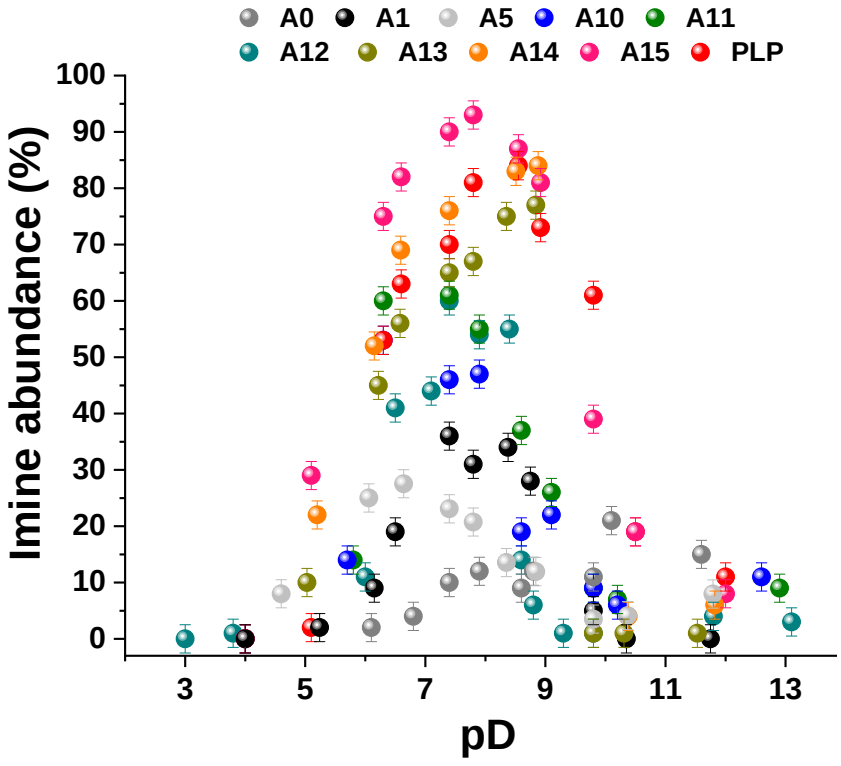

Fig. S6. Imine abundances (%) observed in the reaction between the aldehydes and **B1** at different pD values. Reaction conditions: 5 mM aldehyde and 5 mM **B1**, D_2O, 295 K, 3 h. Error in measurements: 5%.

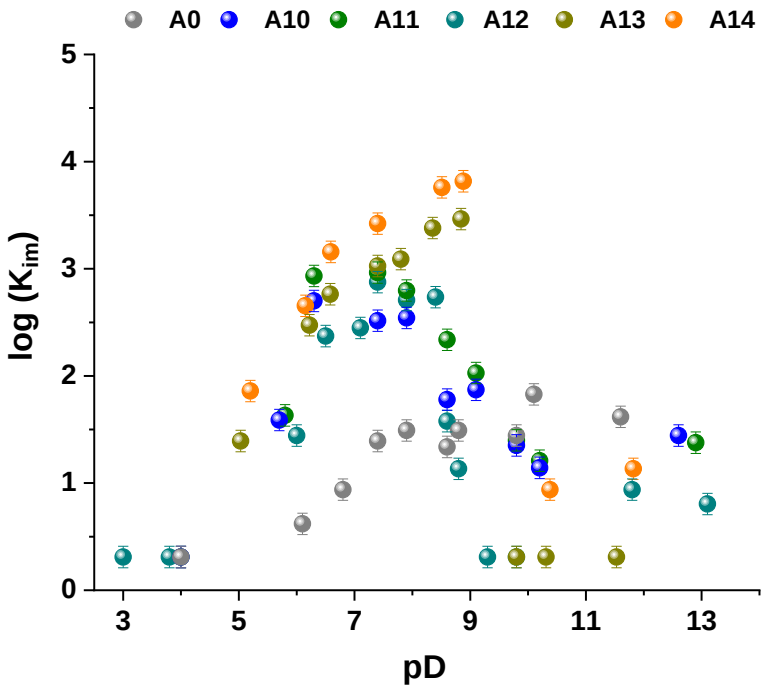

Fig. S7. Hammett plot of the log(K_{im}) for the addition of **B1** to aldehydes **A0**, **A10**, **A11**, **A12, A13** and **A14** at different pD values. Reaction conditions: 5 mM aldehyde and 5 mM **B1**, D_2O, 295 K, 3 h. Error in measurements: 5%.

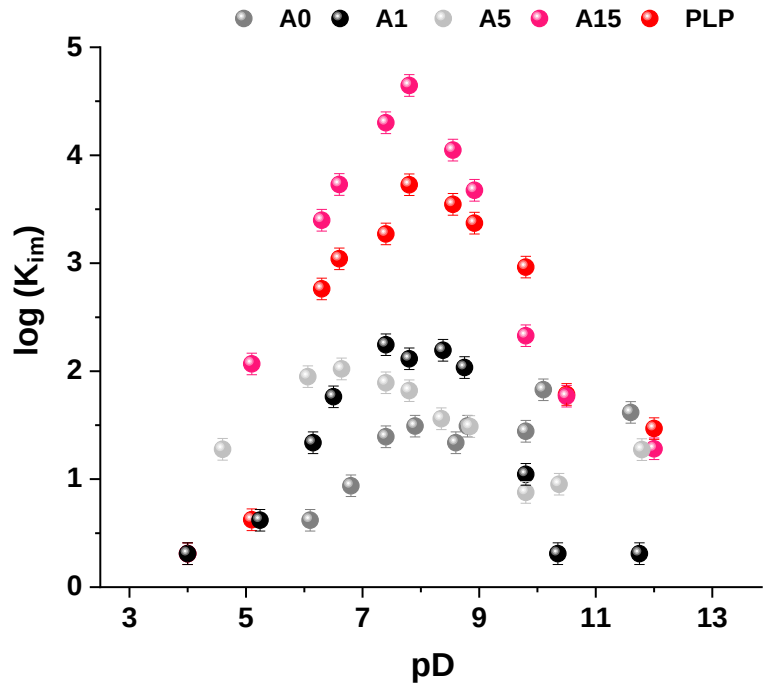

Fig. S8. Hammett plot of the log(K_{im}) for the addition of **B1** to aldehydes **A0**, **A1**, **A5, A15** and **PLP** at different pD values. Reaction conditions: 5 mM aldehyde and 5 mM **B1**, D_2O, 295 K, 3 h. Error in measurements: 5%.

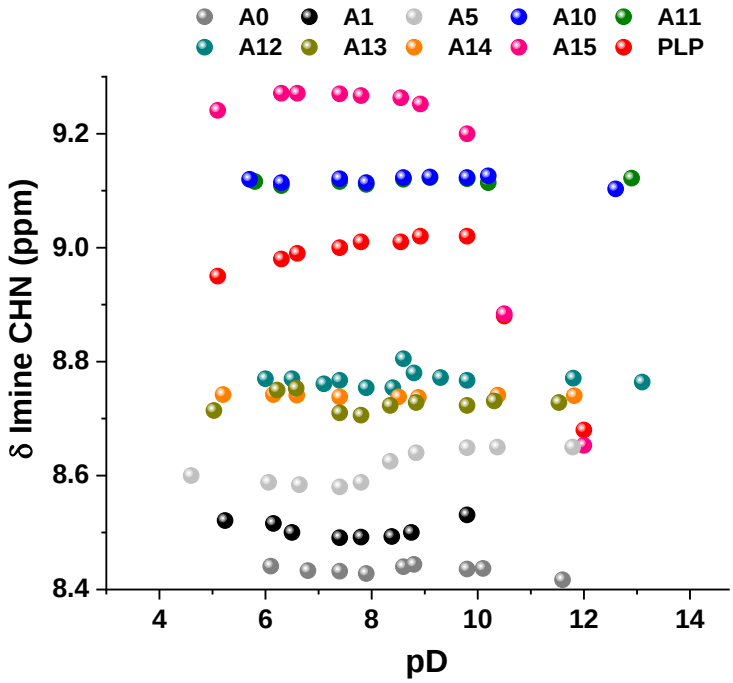

Fig. S9. pD evolution of the ^{1}H-NMR (500 MHz, D_2O, 295 K) shifts for the -CH=N- (or -CH=N^{+}H-) signals of the products of the condensation reaction between **B1** and the different aldehydes. Reaction conditions: 5 mM aldehyde and 5 mM **B1**, D_2O, 295 K, 3 h. Error in measurements: 5%.

Table S2. Individual sulfonate n→π* and n→σ* interactions (kcal/mol) in **A12, A12B1** and **A12B1** iminium.

Species	n→π* (Kcal/mol)	n→σ* (Kcal/mol)	**Sum (Kcal/mol)**
A12	0.8	-	**9.9**
	4.3		
	0.8		
	4.0		
A12B1 imine	0.5	-	**5.5**
	2.5		
	2.5		
A12B1 iminium	2.9	6.5 (N-H)	**33.0**
		22.3 (N-H)	
		1.3 (C-H)	

Table S3. Calculated pKa and protonation degree for the terminal amino groups of the different nucleophiles studied.

Amine	pKa[a]	Unprotonated -NH_2 (%)[a,b]
B1	7.9	75
ValOMe	7.5	46
B2[c]	9.5	20
B3	9.1	2
B4	9.6	1
Val	9.6	1
B5	10.2	0.16
LysOMe Nα	7.4	50
LysOMe Nε	10.2	0.16
Lys Nα	9.4	1
Lys Nε	10.3	0.14
AcNαLysOMe Nε	10.2	0.16

[a] Values calculated using MarvinSketch. [b] Values determined at pD = 7.0 (pH = 7.4). [c] The unprotonation degree of **B2** would be higher when the vicinal tertiary amino group is protonated.

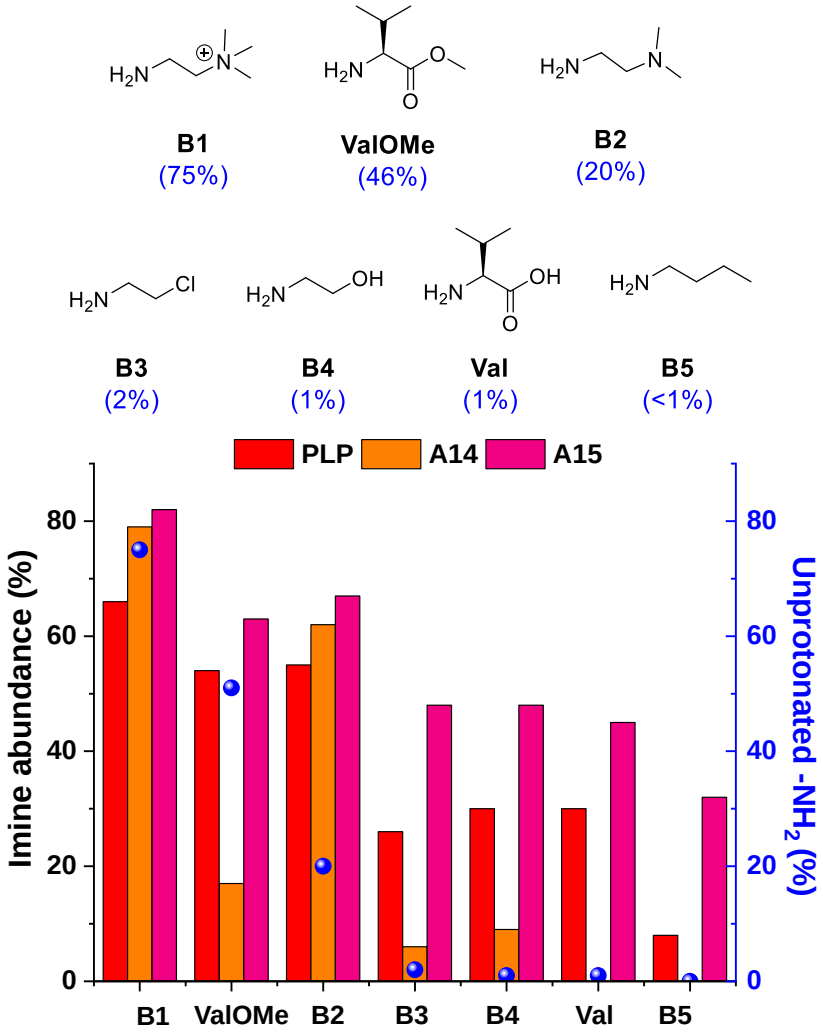

Fig. S10. Chemical structures (above) and imine abundances (below) for the amine screening using **PLP**/**A14**/**A15**. Imine abundances determined by ^{1}H NMR spectroscopy (500 MHz, D_2O, pD 7.0, 50 mM PBS, 295 K). Concentration: 5 mM for each component. The numbers in brackets correspond to the unprotonated -NH_2 group at pD 7.0. See Table S3 for pKa and protonation degree of amines.

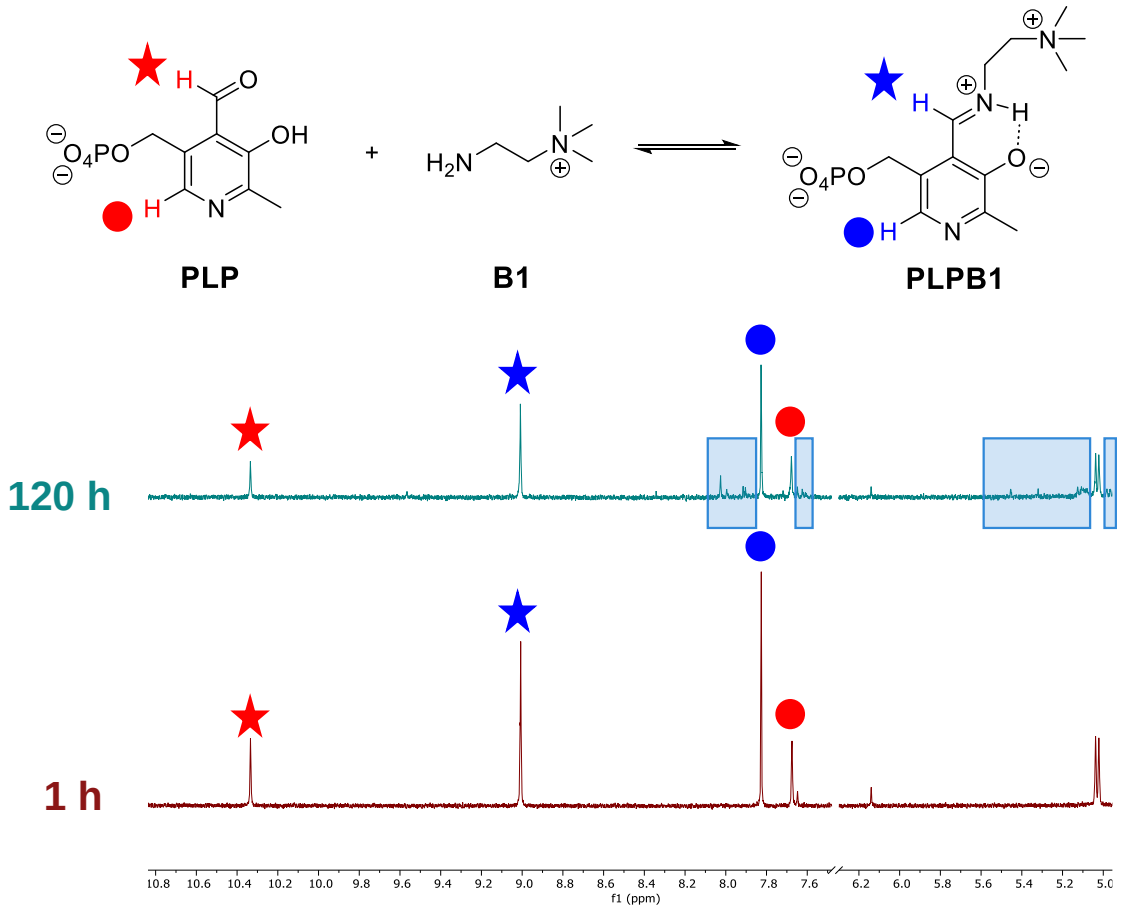

Fig. S11. Time evolution of the ^{1}H NMR spectrum (400 MHz, D_2O, pD 7.0, 50 mM PBS, 295 K) for the reaction between **PLP** and **B1** (5 mM each). Signals assigned to side-products have been highlighted with blue squares. Most characteristic peaks for the aldehyde and iminium have been highlighted in red and blue, respectively.

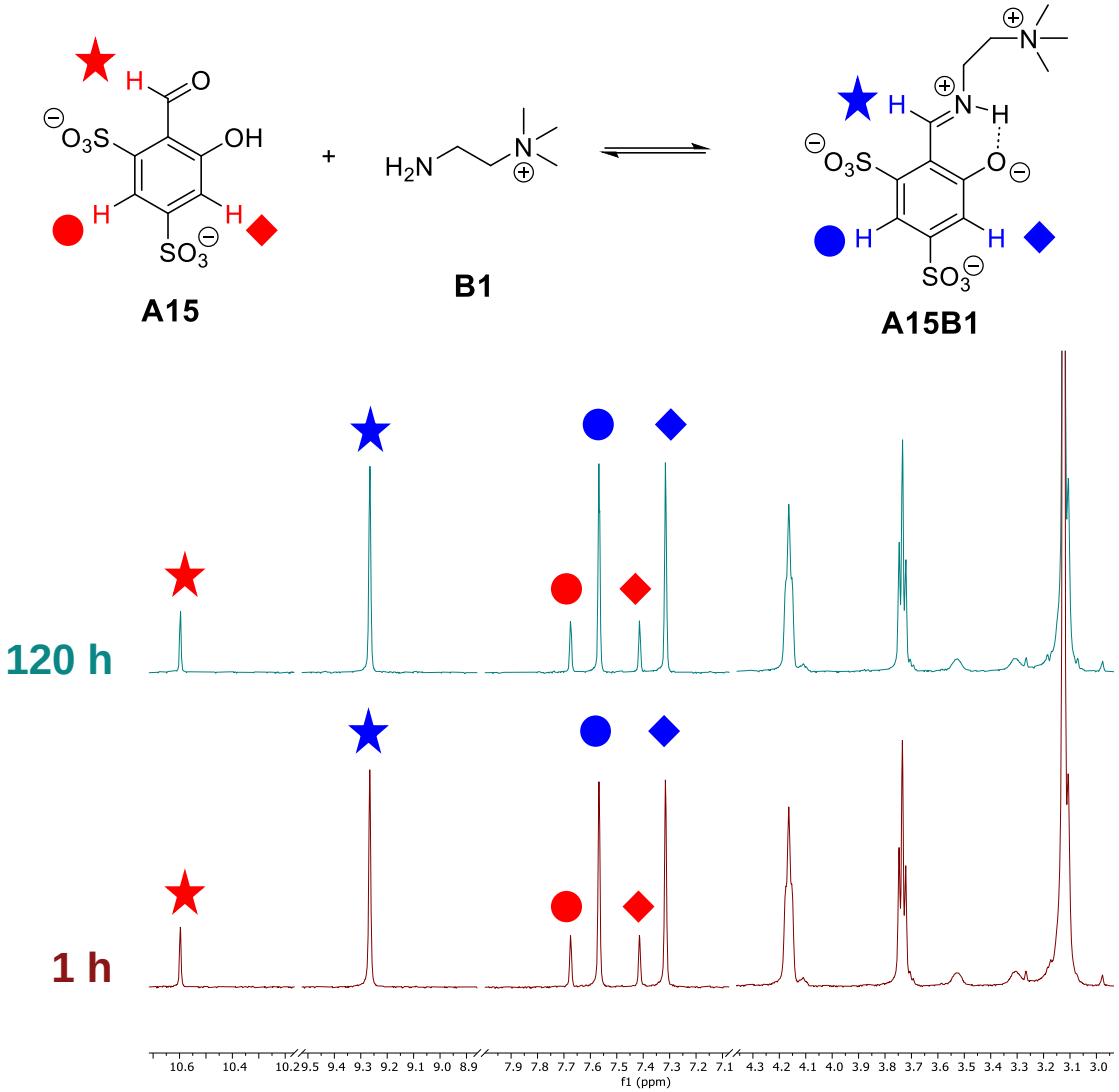

Fig. S12. Time evolution of the ^{1}H NMR spectrum (500 MHz, D_2O, pD 7.0, 50 mM PBS, 295 K) for the reaction between **A15** and **B1** (5 mM each). Most characteristic peaks for the aldehyde and iminium have been highlighted in red and blue, respectively.

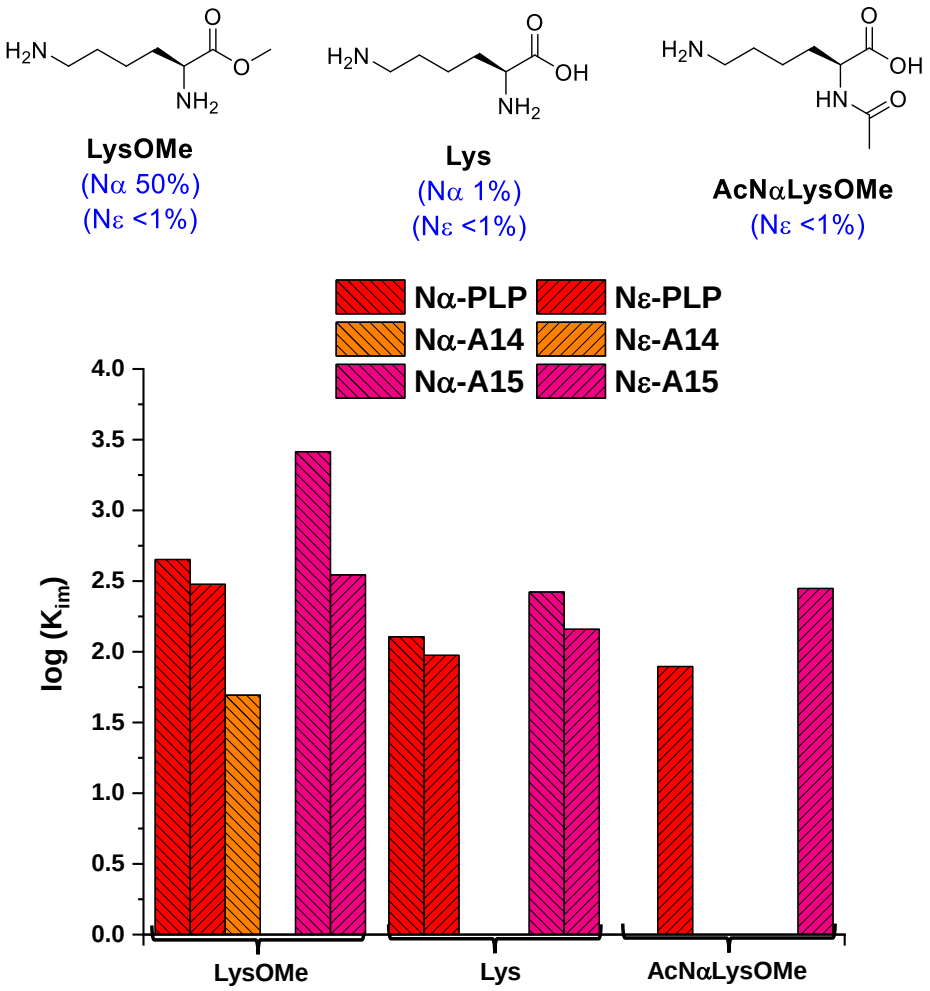

Fig. S13. Chemical structures (above) and log K_{im} (below) for the reaction between **PLP**/**A4**/**A15** and Lys derivatives: **LysOMe**, **Lys**, and **AcNαLysOMe**. Component abundances determined by ^{1}H NMR spectroscopy (500 MHz, D_2O, pD 7.0, 50 mM PBS, 295 K). Concentration: 5 mM for each component. The numbers in brackets correspond to the unprotonated -NH_2 group at pD 7.0. See Table S3 for pKa and protonation degree of amines.

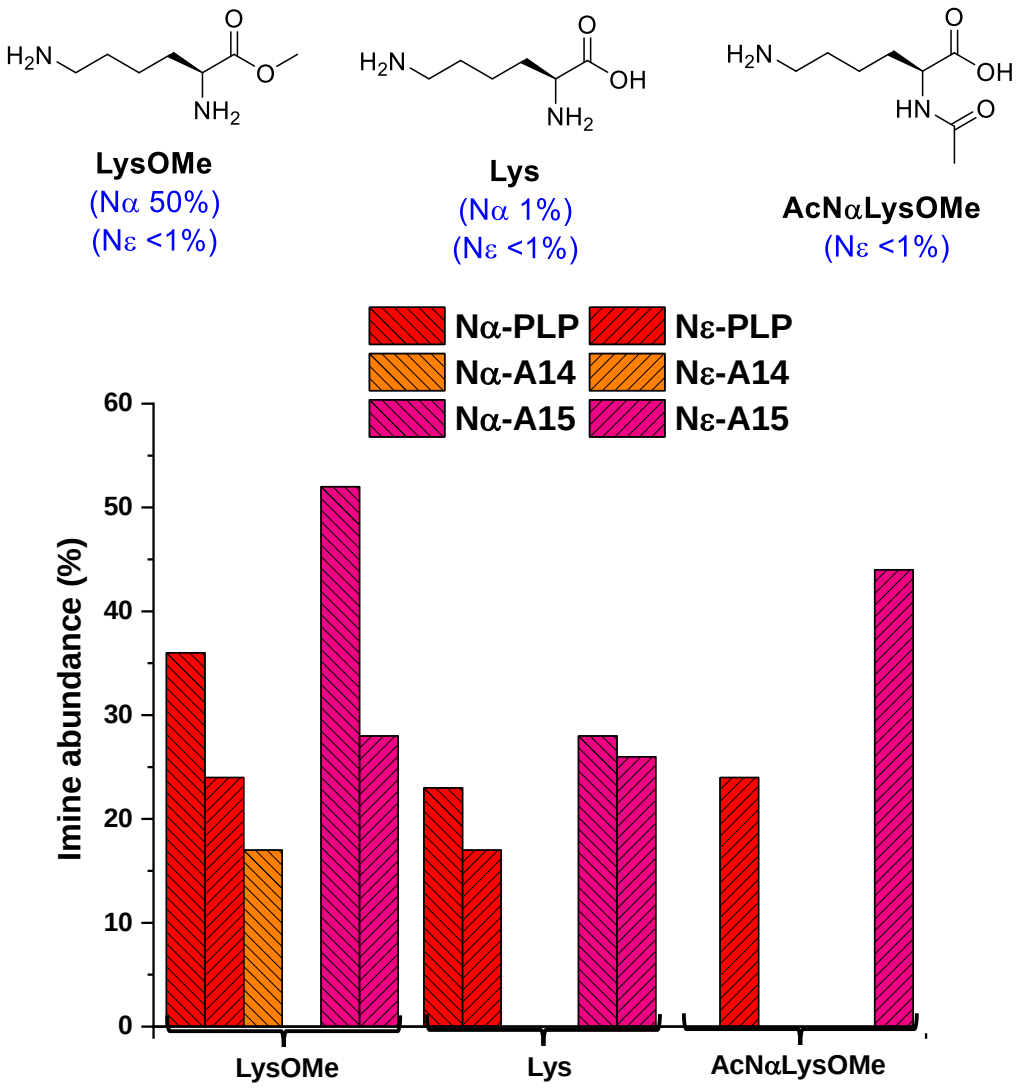

Fig. S14. Chemical structures (above) and imine abundances (below) for the reaction between **PLP**/**A14**/**A15** and Lys derivatives: **LysOMe**, **Lys**, and **AcNαLysOMe**. Imine abundances (%) determined by ^{1}H NMR spectroscopy (500 MHz, D_2O, pD 7.0, 50 mM PBS, 295 K). Concentration: 5 mM for each component. The numbers in brackets correspond to the unprotonated -NH_2 group at pD 7.0. See Table S3 for pKa and protonation degree of amines.

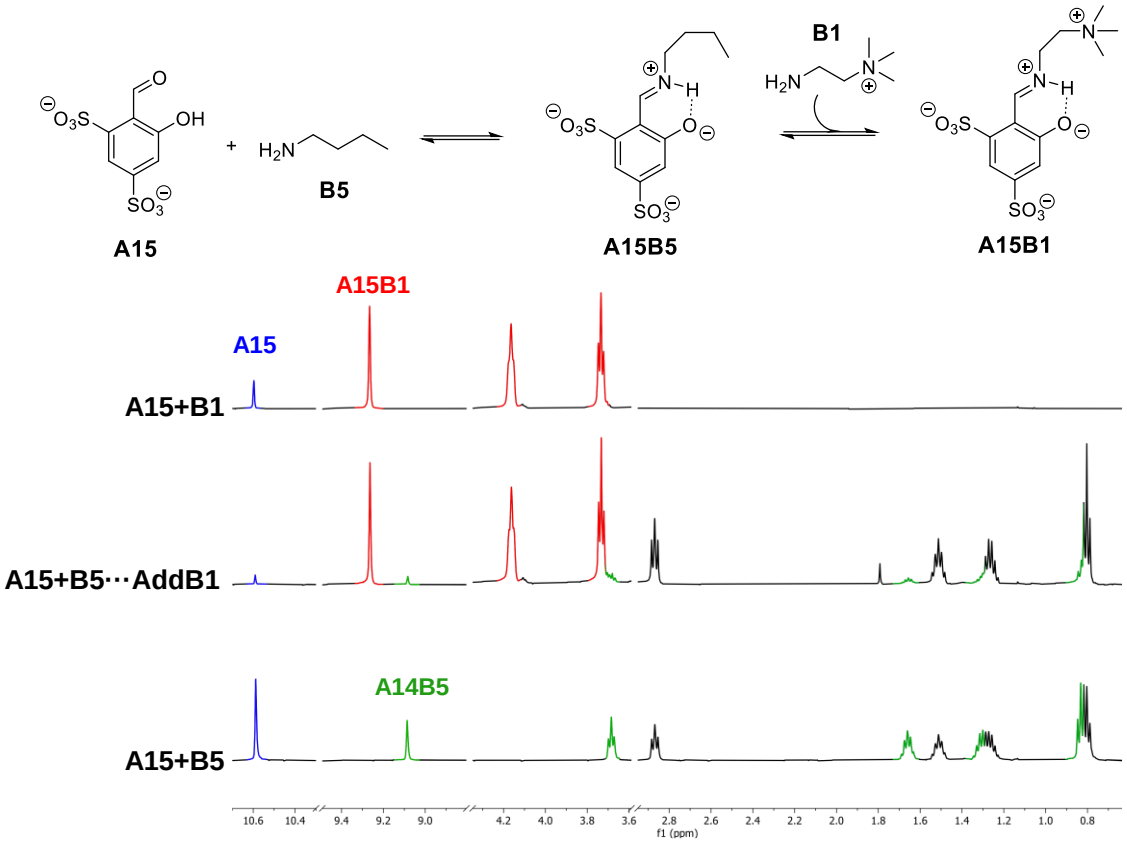

Fig. S15. ^{1}H NMR (500 MHz, D_2O, pD 7.0, 50 mM PBS, 295 K) monitoring of the dynamic transimination rearrangement between initially formed **B5A15** and **B1**. Final concentration: 5 mM solution in **A15**/**B1**/**B5**. Signals corresponding to **A14** have been highlighted in blue, to **A15B5** in green and to **A15B1** in red. The spectra of separated reactions between **A15**/**B1** (above) and **A15**/**B5** (below) have also been introduced for comparison.

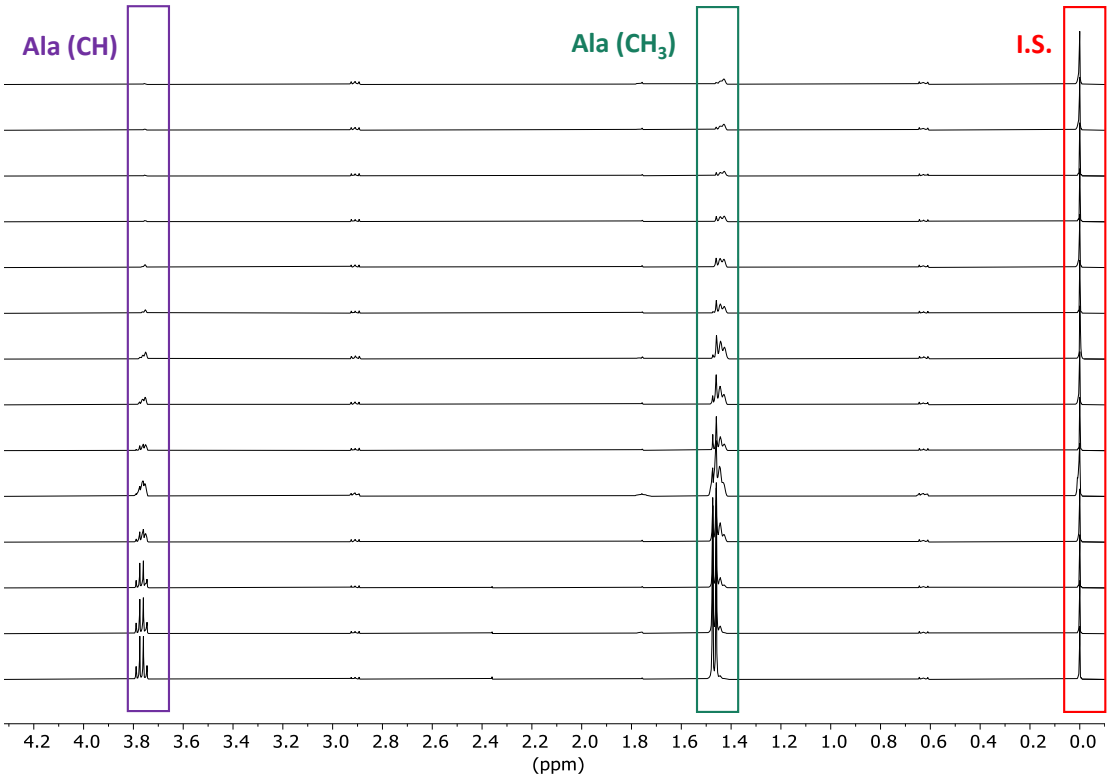

Fig. S16. ^{1}H NMR (500 MHz, D_2O, pD 7.8, 100 mM PBS, 295 K) monitoring of the L-alanine-D_2O exchange reaction. Time increases from below (t1= 5 min) to above (tf= 28 h). Conditions: L-alanine (90 mM), pyruvate (1.5 mM), potassium phosphate buffer (100 mM, pD 7.8) and 7 units of **GPT** (*ca.* 1 µM).

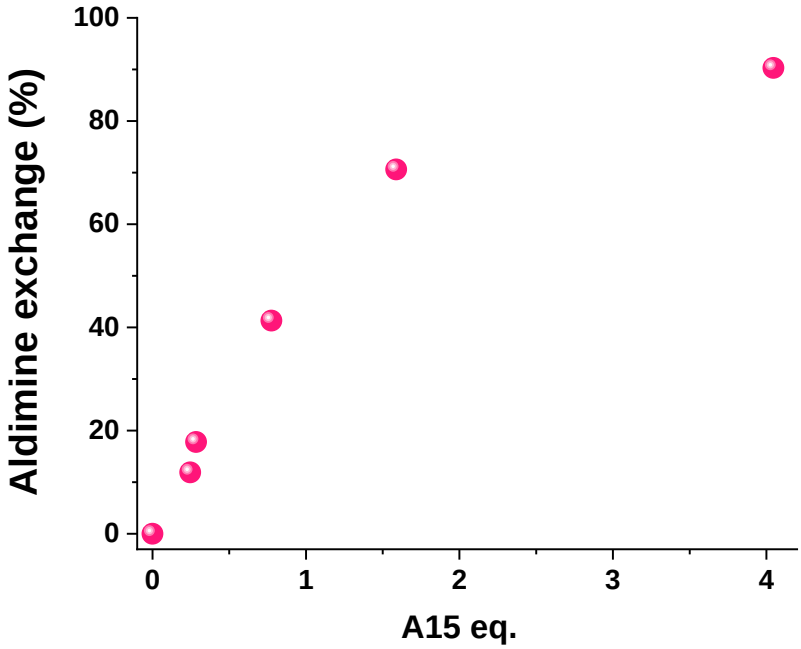

Fig. S17. Results for the aldimine exchange reaction between the preformed **PLPAcNαLysOMe**and increasing amounts of **A15**. The exchange (%) has been calculated by ^{1}H NMR (500 MHz, D_2O, pD 7.8, 100 mM PBS, 295 K) after 3 h of equilibration.

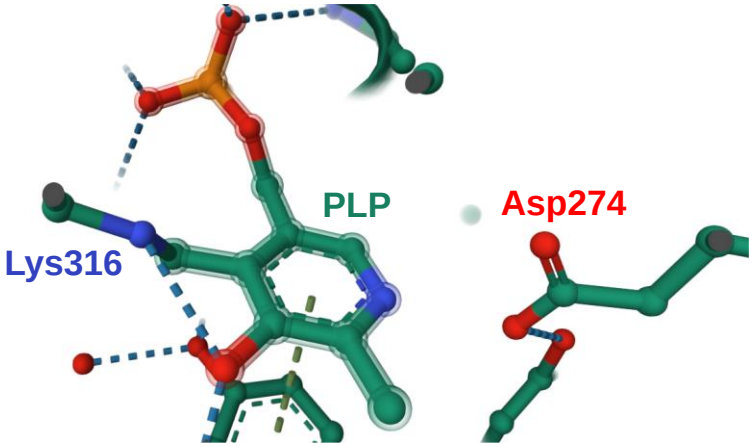

Fig. S18. PLP-aldimine-complex with an analogous protein (Human alanine aminotransferase 2, PDB: 3IHJ) showing the supramolecular interactions between the cofactor and the amino acid residues of the sophisticated active pocket.

3. Example of imine yield calculation

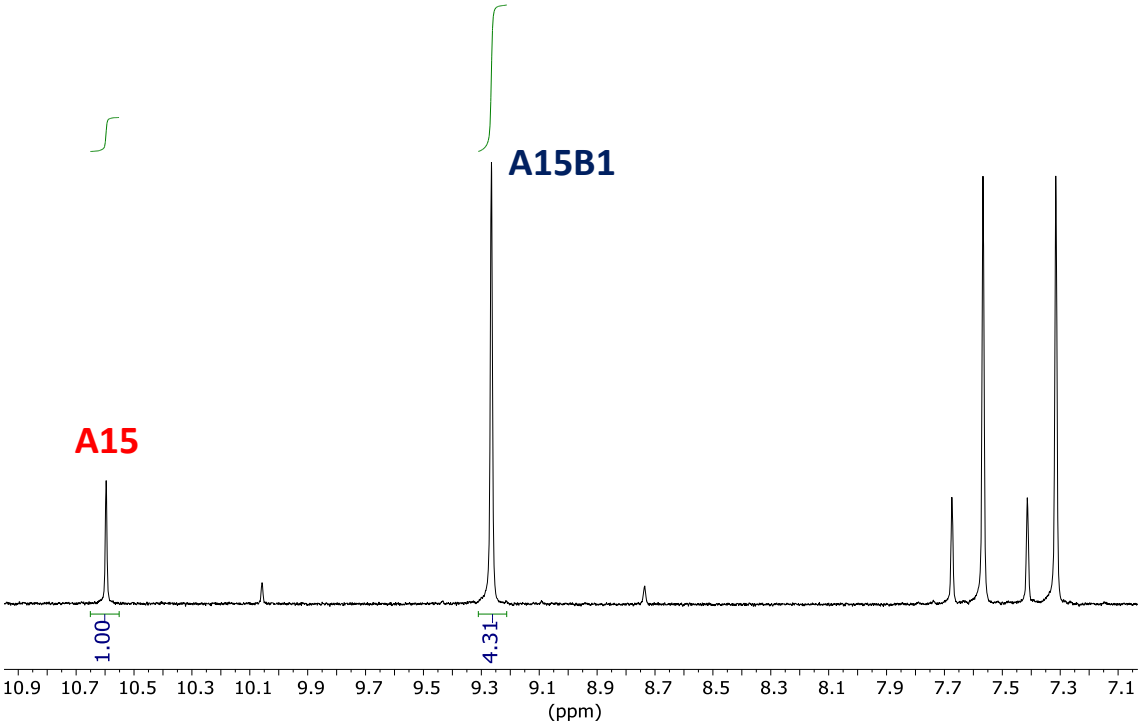

Fig. S19. Selected example for the product abundance quantification using ^{1}H-NMR spectrum (500 MHz, D_2O + phosphate buffer 50mM, pD 7.0, 295 K). The crude corresponds to the condensation reaction between **A15** and **B1** (5 mM each) after 1 h of equilibration. In this case, the imine yield would be 82%.

4. Characterization

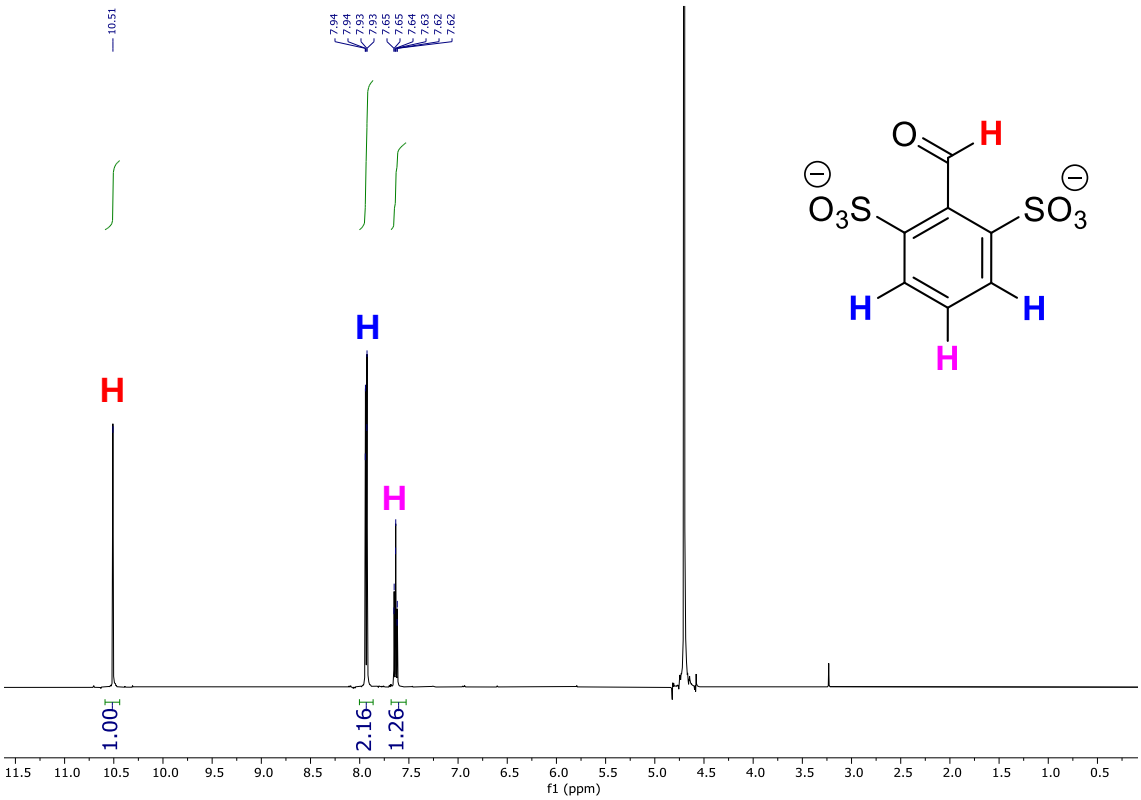

Fig. S20. ^{1}H-NMR spectrum (500 MHz, D_2O, 295 K) of **A12**.

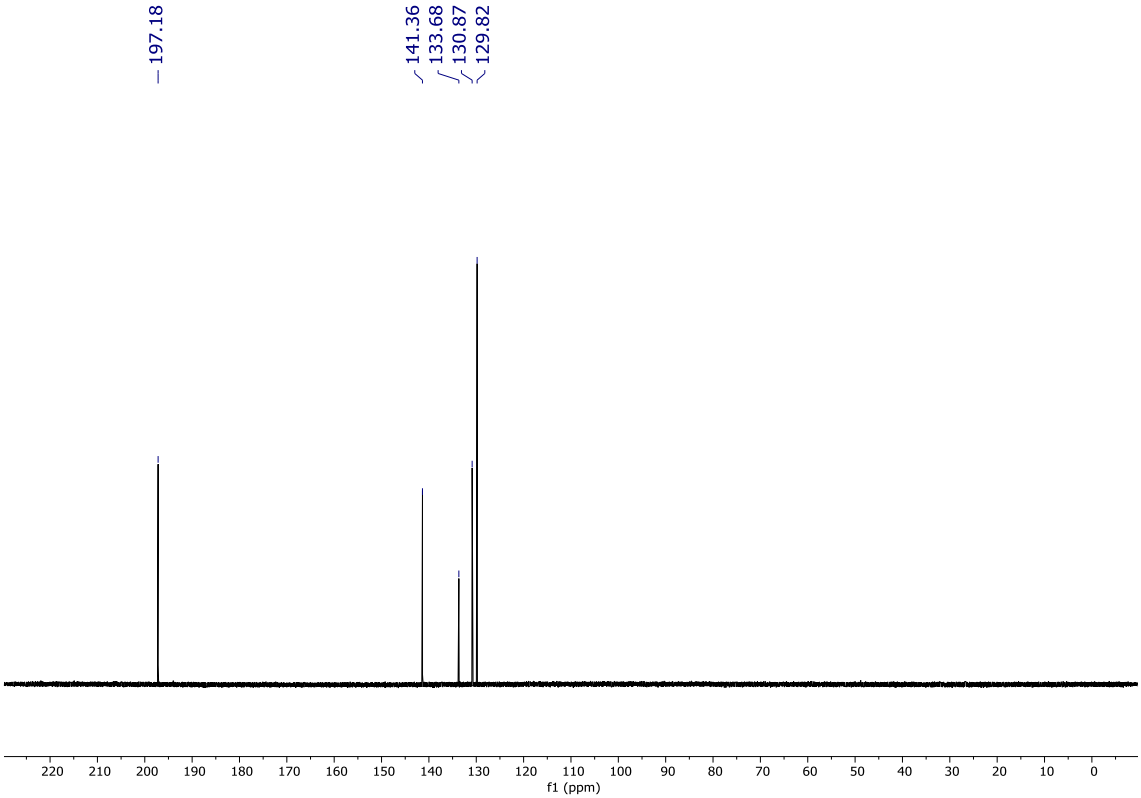

Fig. S21. ^{13}C{^{1}H}-NMR spectrum (126 MHz, D_2O, 295 K) of **A12**.

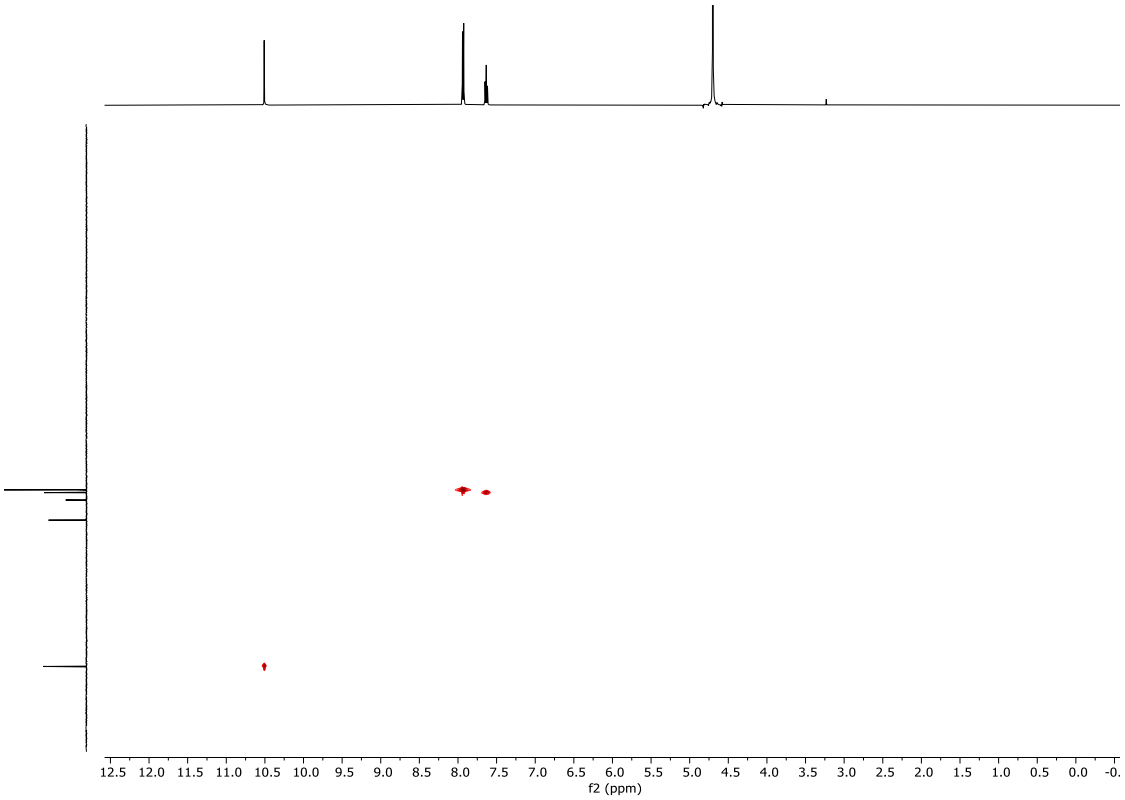

Fig. S22. HSQC-NMR spectrum (500 MHz, D_2O, 295 K) of **A12**.

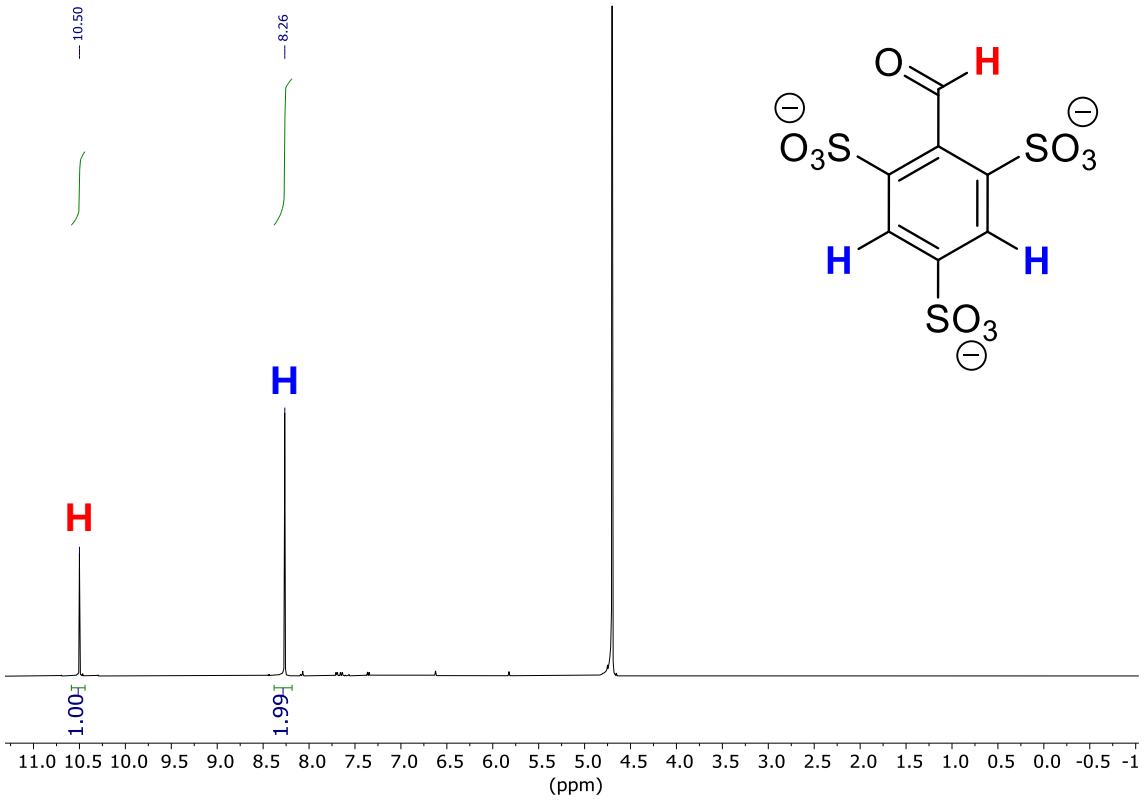

Fig. S23. ^{1}H-NMR spectrum (500 MHz, D_2O, 295 K) of **A13**.

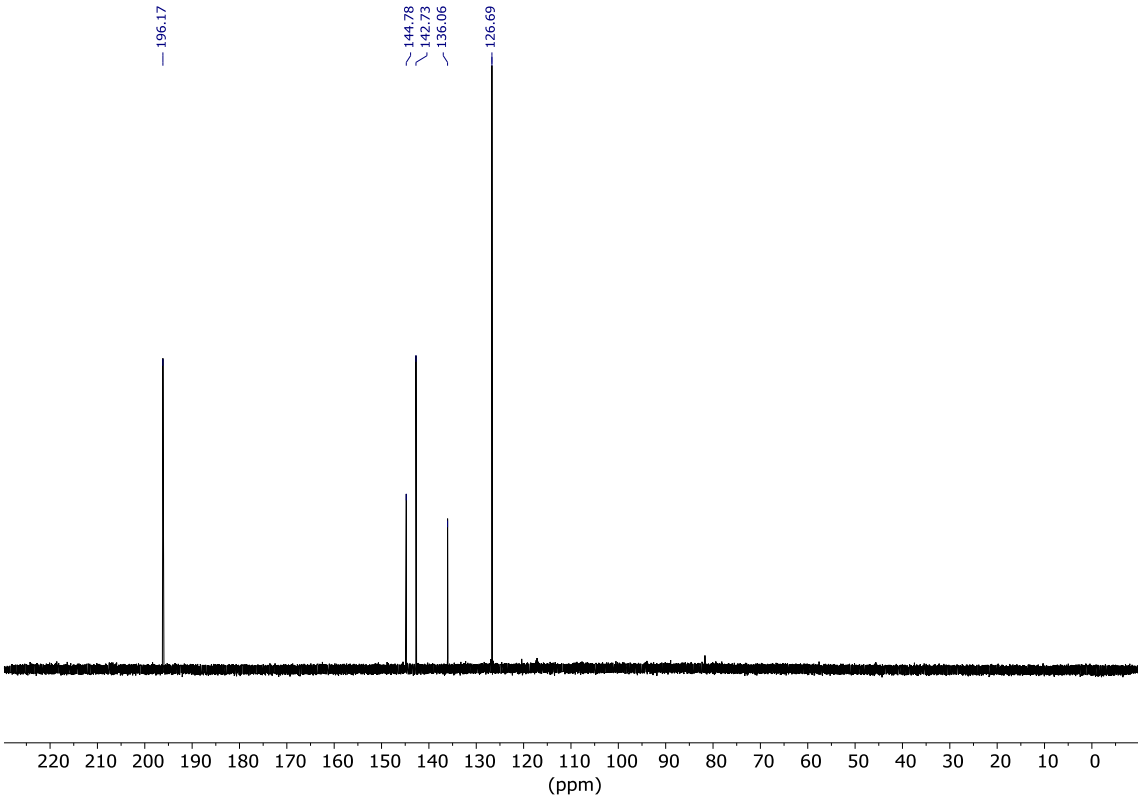

Fig. S24. $^{13}C\{^{1}H\}$-NMR spectrum (126 MHz, D_2O, 295 K) of **A13**.

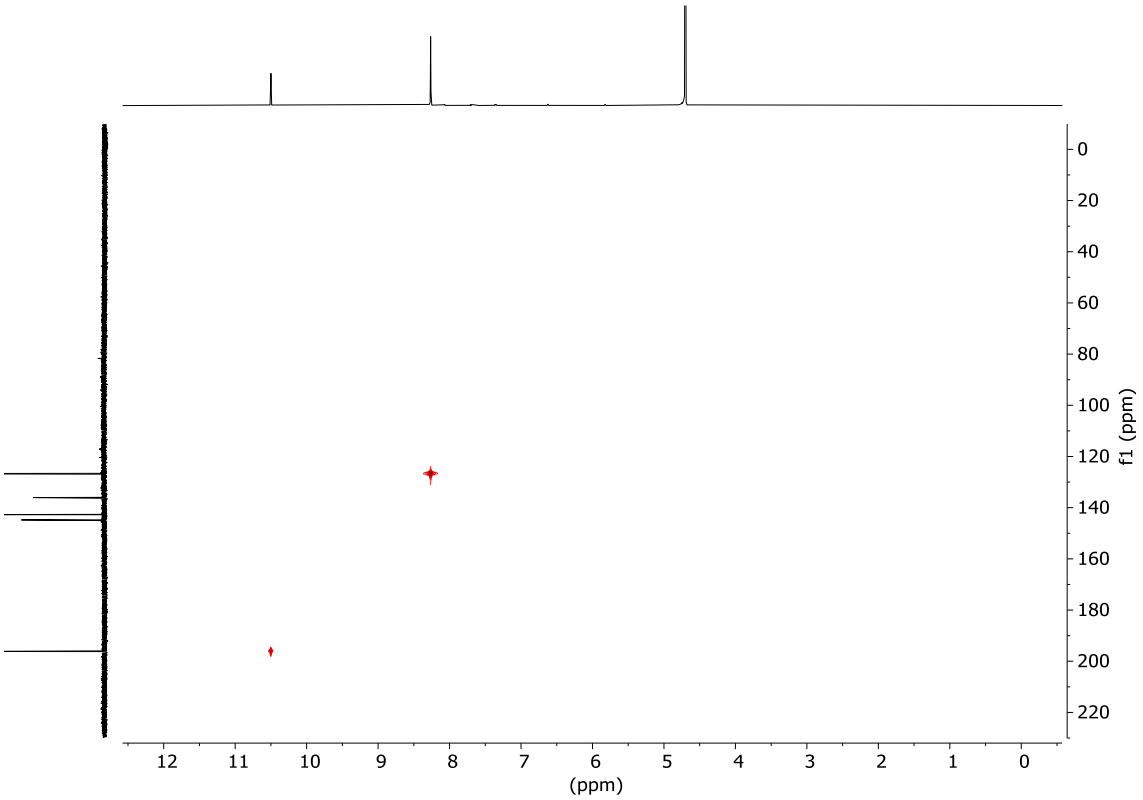

Fig. S25. HSQC-NMR spectrum (500 MHz, D_2O, 295 K) of **A13**.

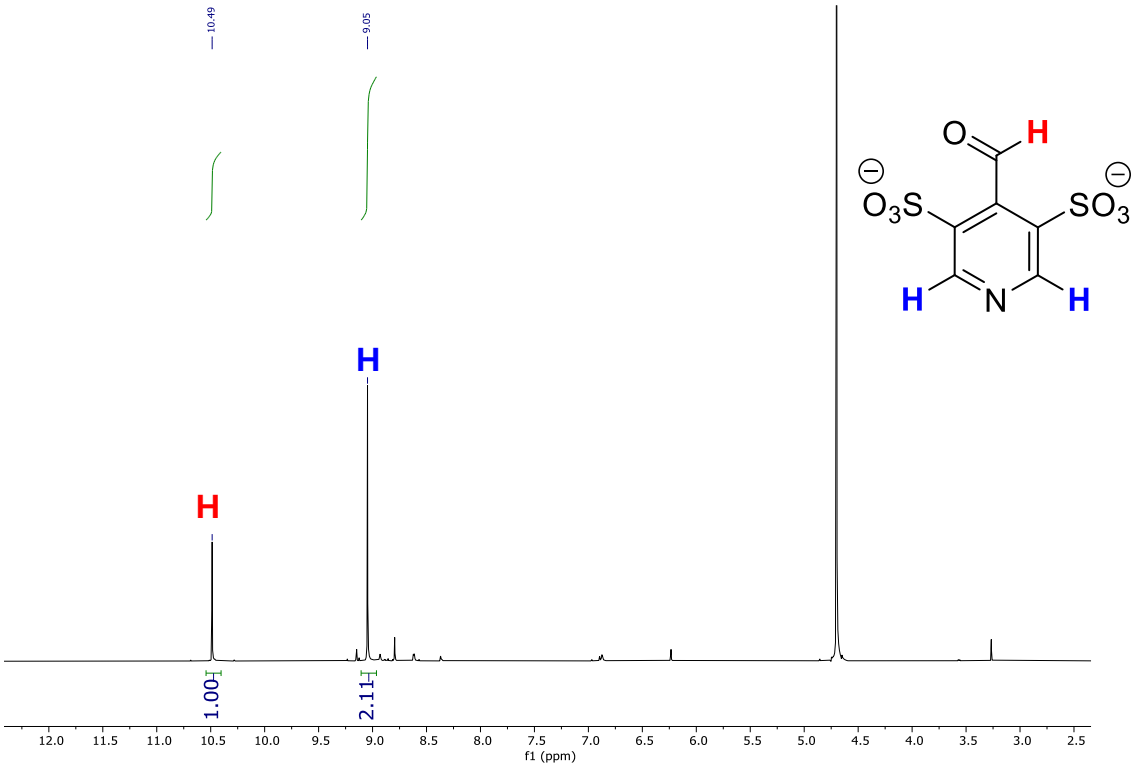

Fig. S26. ^{1}H-NMR spectrum (500 MHz, D_2O, 295 K) of **A14**.

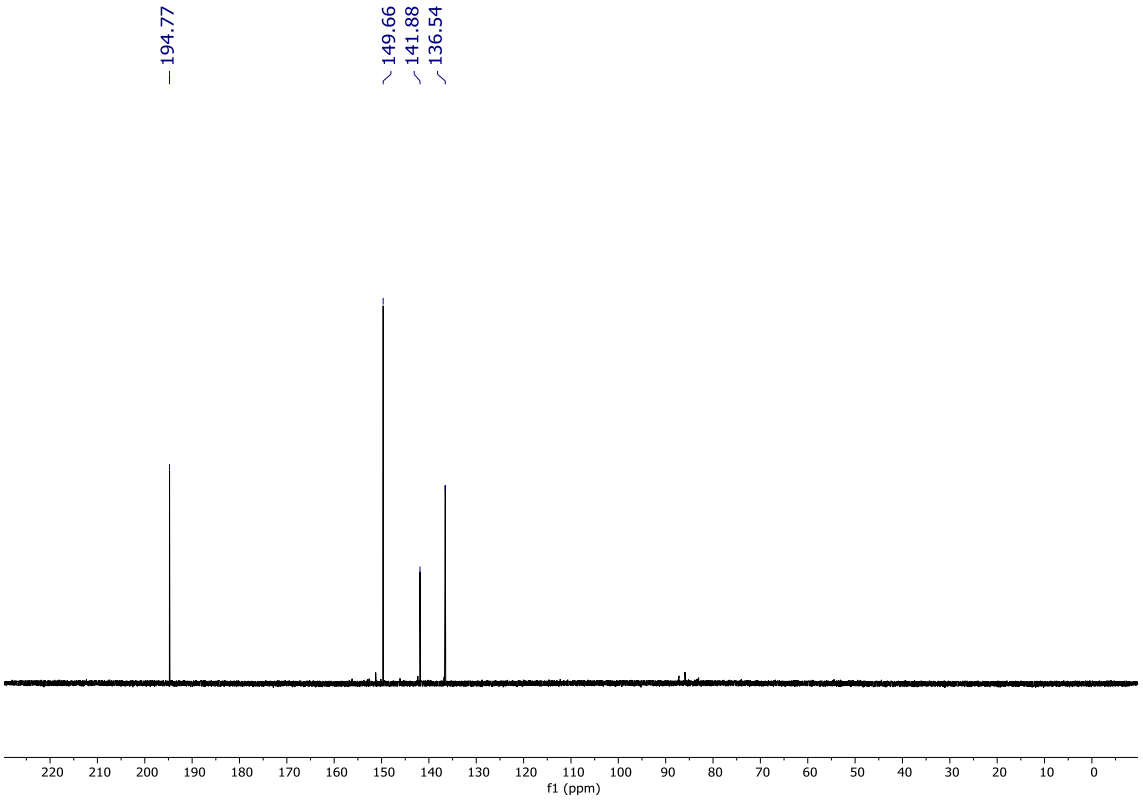

Fig. S27. ^{13}C{^{1}H}-NMR spectrum (126 MHz, D_2O, 295 K) of **A14**.

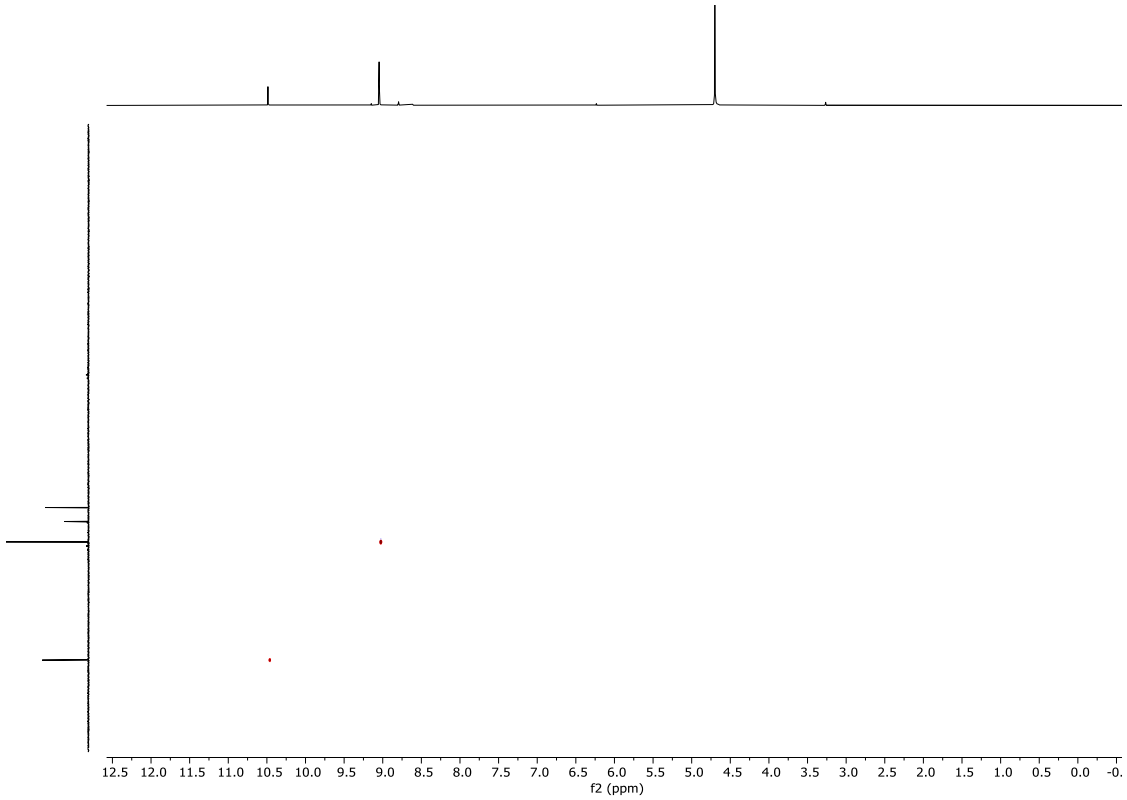

Fig. S28. HSQC-NMR spectrum (500 MHz, D_2O, 295 K) of **A14**.

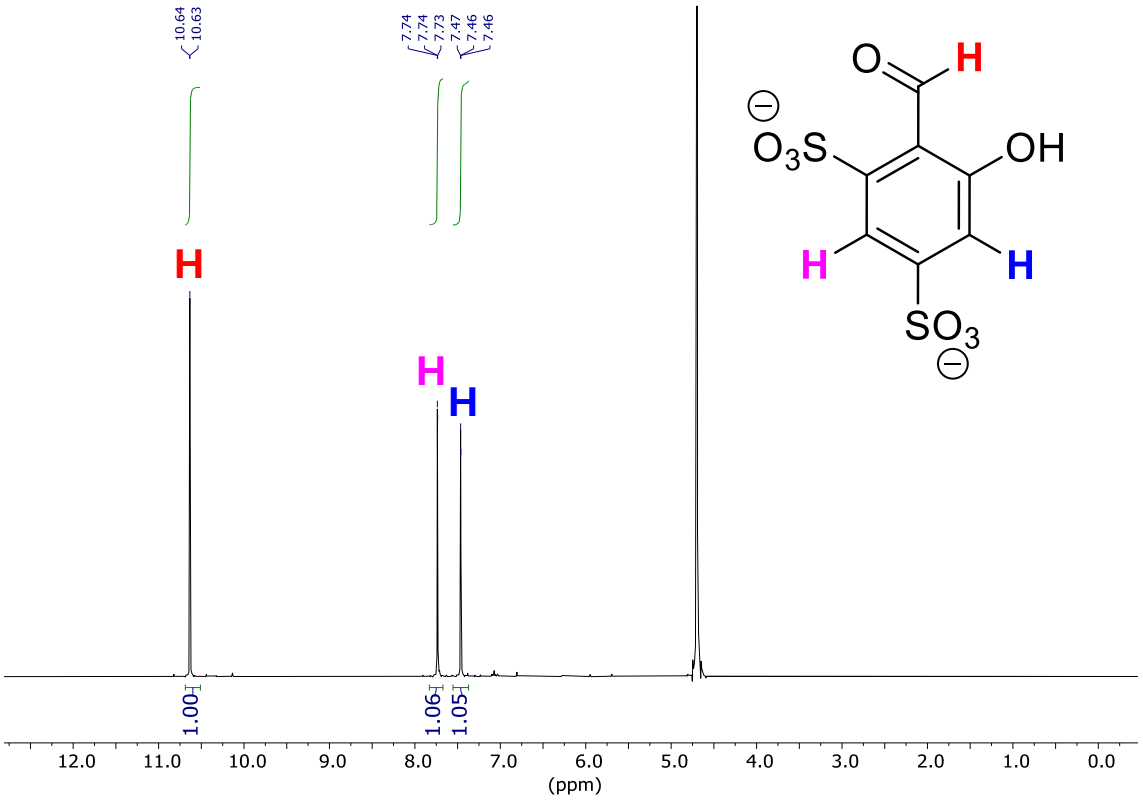

Fig. S29. ^{1}H-NMR spectrum (500 MHz, D_2O, 295 K) of **A15**.

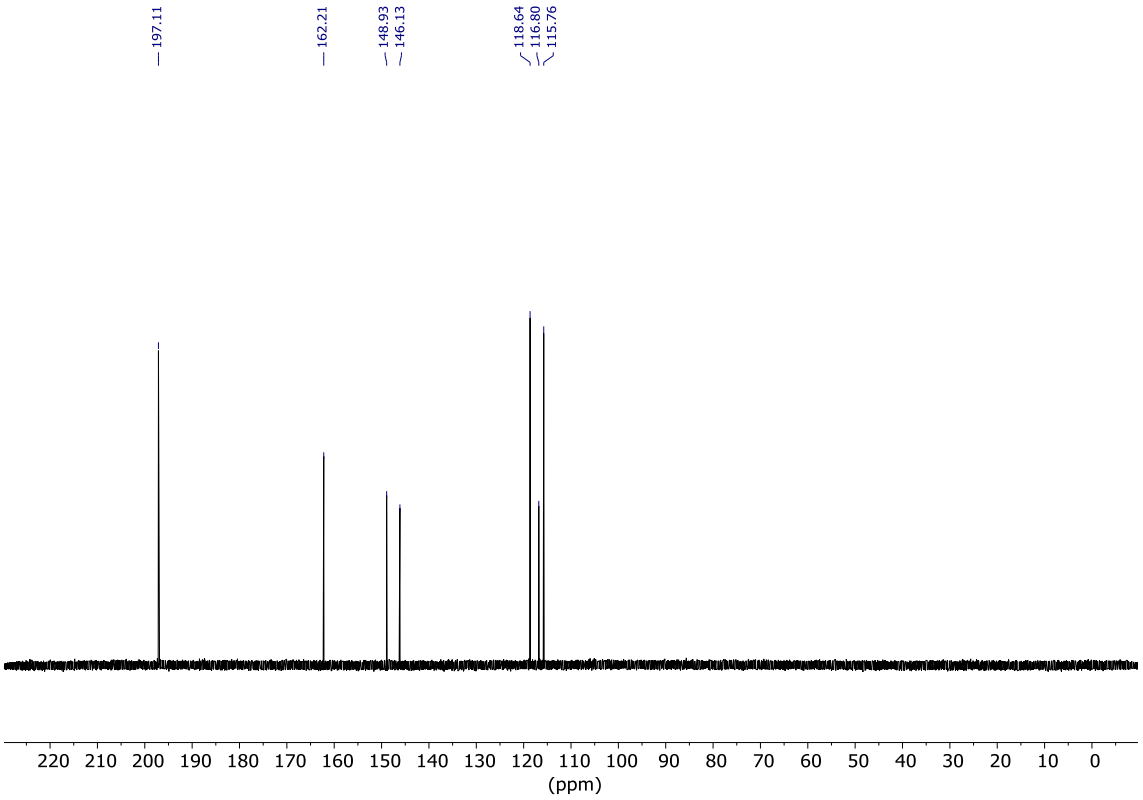

Fig. S30. $^{13}C\{^{1}H\}$-NMR spectrum (126 MHz, D_2O, 295 K) of **A15**.

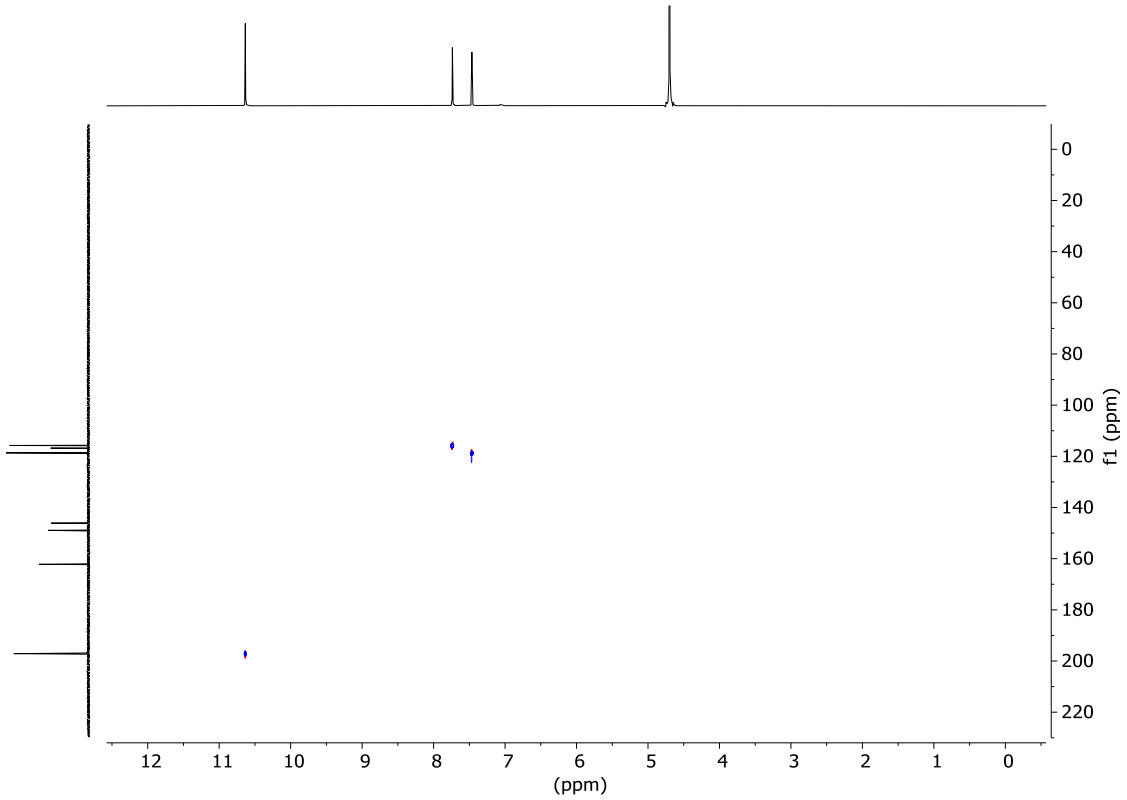

Fig. S31. HSQC-NMR spectrum (500 MHz, D_2O, 295 K) of **A15**.

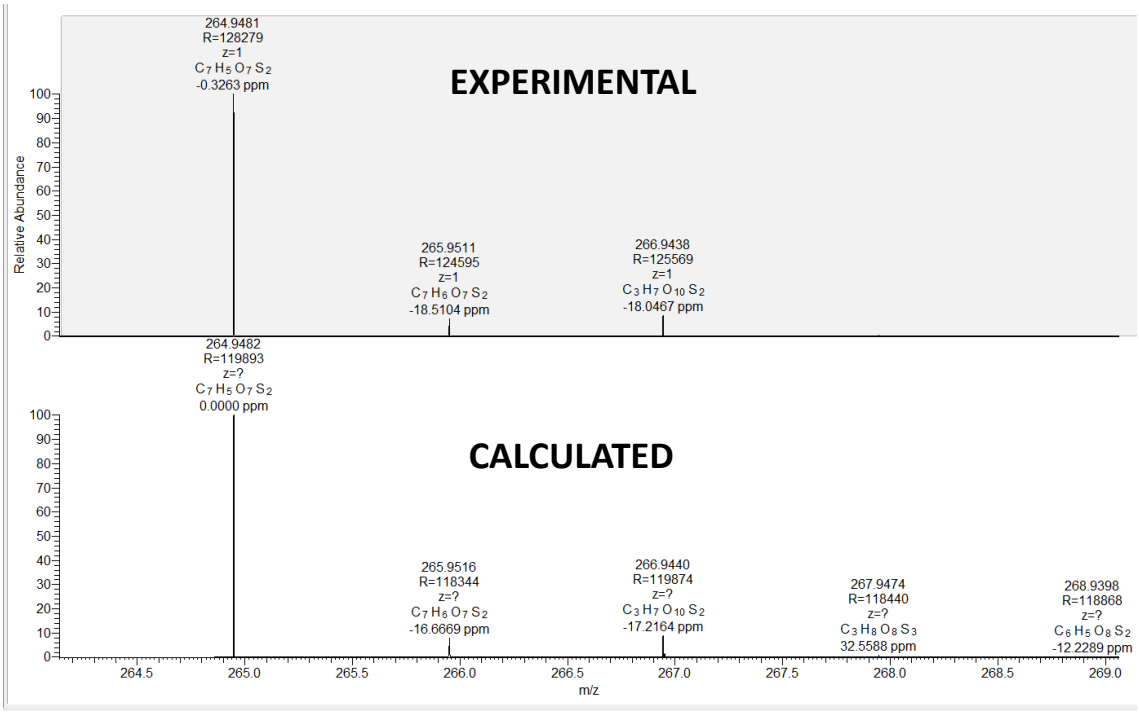

Fig. S32. HRMS-QTOF(-) spectrum (H_2O) of **A12**.

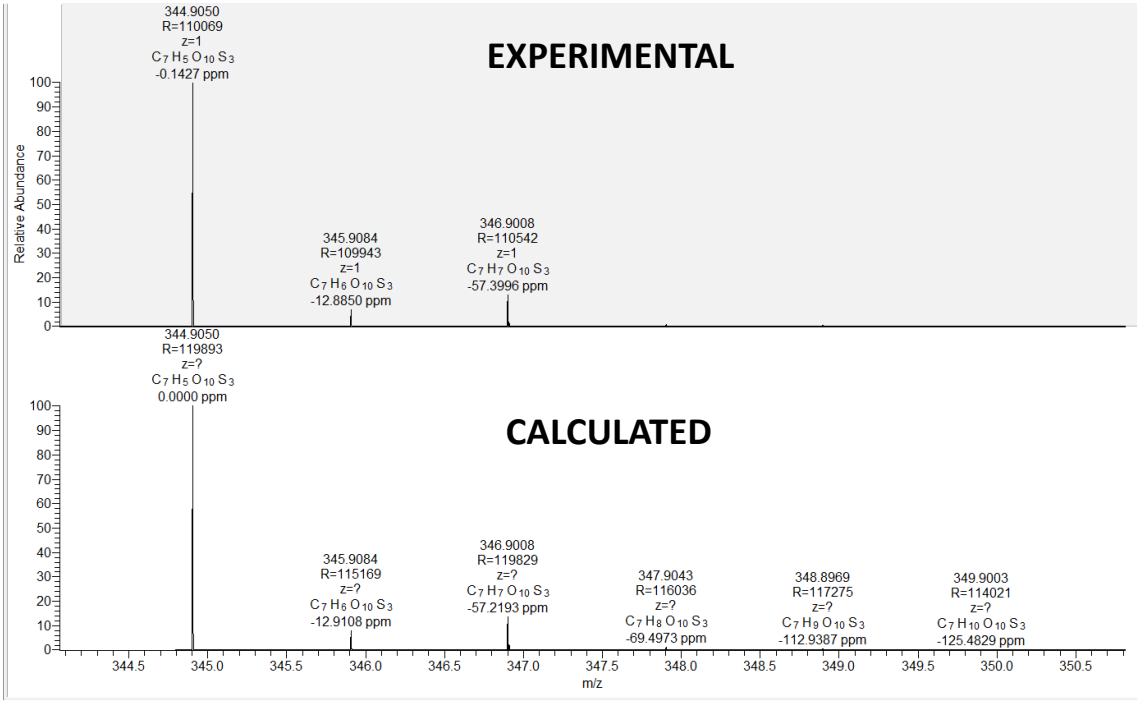

Fig. S33. HRMS-QTOF(-) spectrum (H_2O) of **A13**.

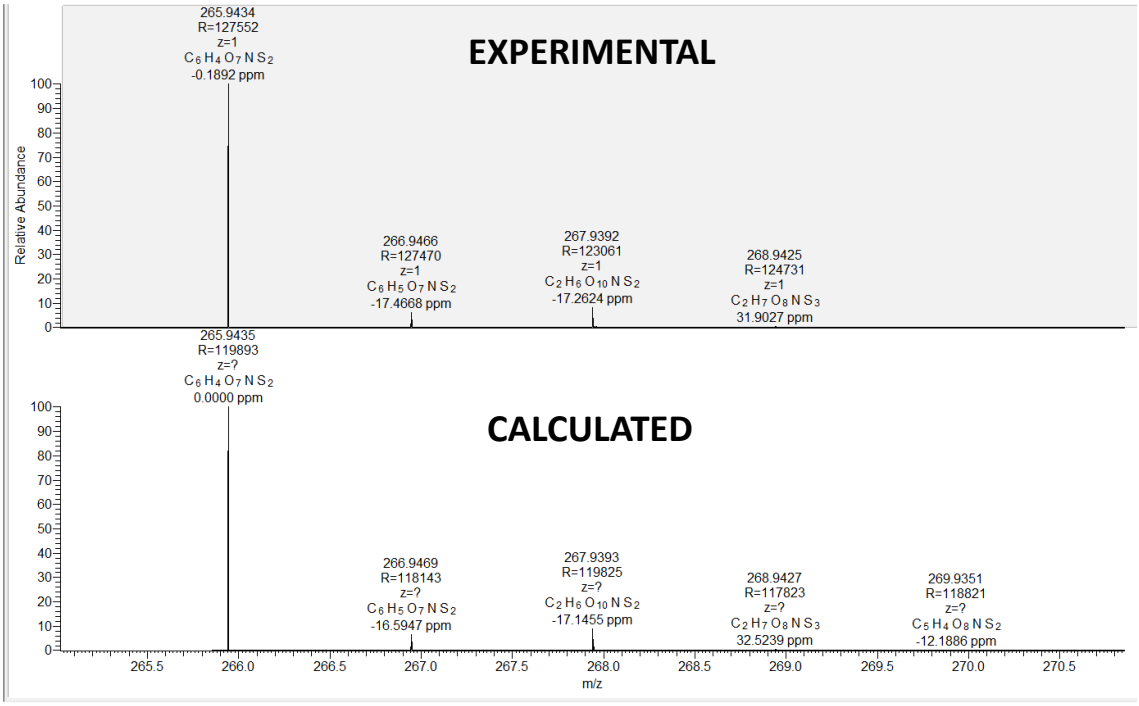

Fig. S34. HRMS-QTOF(-) spectrum (H_2O) of **A14**.

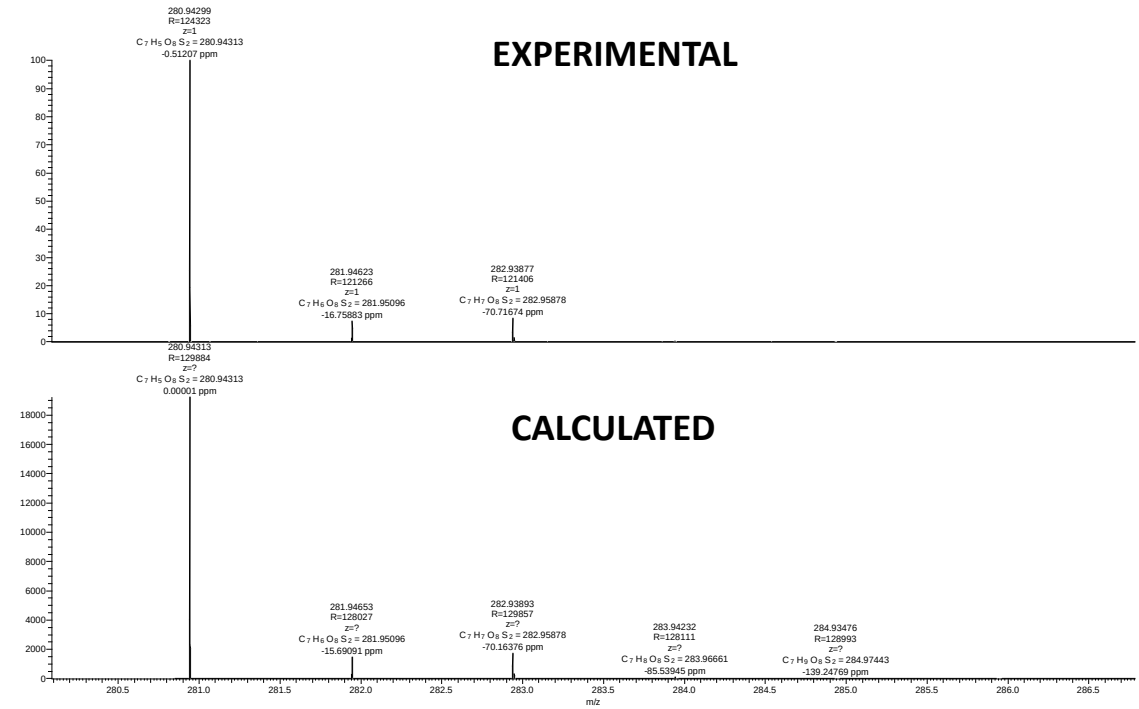

Fig. S35. HRMS-QTOF(-) spectrum (H_2O) of **A15**.

5. DFT details

- Lowest energy conformation for **H_2O**.

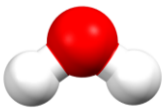

Cartesian coordinates (3 atoms), E (298.15 K) = -76.45170 Hartree

1	O	-2.5310	-1.4669	0.0000
2	H	-1.5710	-1.4669	0.0000
3	H	-2.8514	-0.5620	0.0000

- Lowest energy conformation for **$B1^+$**.

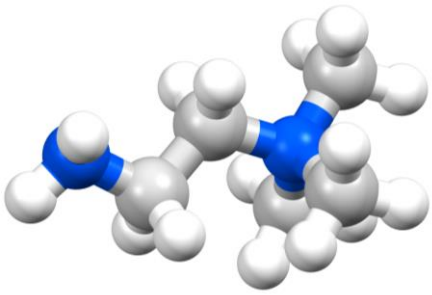

Cartesian coordinates (22 atoms), E (298.15 K) = -308.83021 Hartree

1	C	-2.6725	1.3042	0.1283
2	H	-2.4133	1.7281	1.0997
3	H	-2.2695	1.9708	-0.6432
4	C	-2.0869	-0.1032	0.0000
5	H	-2.4229	-0.7115	0.8389
6	H	-2.4292	-0.5720	-0.9233
7	C	0.0316	0.4588	1.1956
8	H	1.1024	0.2673	1.2007
9	H	-0.1479	1.5295	1.1542
10	H	-0.4300	0.0316	2.0833
11	C	-0.0072	0.4521	-1.2655
12	H	1.0721	0.3167	-1.2698
13	H	-0.4485	-0.0278	-2.1363
14	H	-0.2448	1.5117	-1.2583
15	C	-0.1911	-1.6547	-0.0287
16	H	0.8920	-1.7386	-0.0822
17	H	-0.5582	-2.1135	0.8866
18	H	-0.6465	-2.1286	-0.8955
19	N	-4.1309	1.1541	0.0722
20	H	-4.5713	2.0035	0.4100
21	H	-4.4304	1.0429	-0.8924
22	N	-0.5653	-0.1940	-0.0237

- Lowest energy conformation for **B1-H^{+2}**.

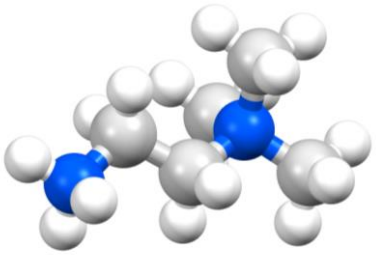

Cartesian coordinates (23 atoms), E (298.15 K) = -309.25826 Hartree

1	C	-2.6646	1.2575	0.1387
2	H	-2.4342	1.7215	1.0942
3	H	-2.3447	1.9124	-0.6674
4	C	-2.087	-0.153	0.0202
5	H	-2.3987	-0.764	0.867
6	H	-2.4285	-0.6321	-0.8967
7	C	0.0282	0.4563	1.2067
8	H	1.1004	0.2761	1.1964
9	H	-0.1571	1.5266	1.1725
10	H	-0.4176	0.0179	2.0967
11	C	-0.0361	0.4657	-1.2612
12	H	1.0435	0.339	-1.275
13	H	-0.4817	-0.0112	-2.1313
14	H	-0.2748	1.5253	-1.242
15	C	-0.1703	-1.6577	-0.0344
16	H	0.913	-1.7145	-0.102
17	H	-0.5145	-2.1284	0.8835
18	H	-0.6255	-2.1339	-0.8999
19	N	-0.5716	-0.1989	-0.0149
20	H	-4.5687	0.6122	0.8024
21	H	-4.5735	2.1159	0.1312
22	H	-4.4839	0.7908	-0.8396
23	N	-4.1646	1.1805	0.0524

- Lowest energy conformation for **A12^{2-}**.

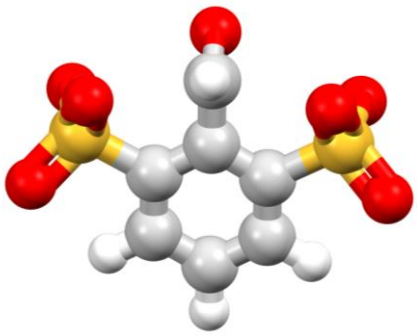

Cartesian coordinates (20 atoms), E (298.15 K) = -1592.51679 Hartree

1	C	0.2876	0.1644	-0.1634
2	C	0.8702	-0.7128	0.7493

3	C	0.0935	-1.6810	1.3781
4	C	0.2649	-1.7706	1.0919
5	C	0.8443	-0.8919	0.1784
6	C	0.0803	0.0945	-0.4582
7	C	0.7140	1.0552	-1.4474
8	O	0.1750	2.1179	-1.1014
9	S	0.6279	-1.0342	-0.1440
10	O	-2.9778	-2.4397	0.1832
11	O	-3.2771	-0.0406	0.7504
12	O	-2.7707	-0.7084	-1.5910
13	S	2.3404	1.4246	-0.9448
14	O	1.8240	1.5264	-2.3387
15	O	3.7235	0.8904	-0.8643
16	O	2.1392	2.6641	-0.1503
17	H	2.9334	-0.6413	0.9387
18	H	1.5477	-2.3701	2.0802
19	H	-0.8829	-2.5317	1.5507
20	H	-0.7213	0.7195	-2.4938

- Lowest energy conformation for the hemiaminal of **A12B1**$^{-}$.

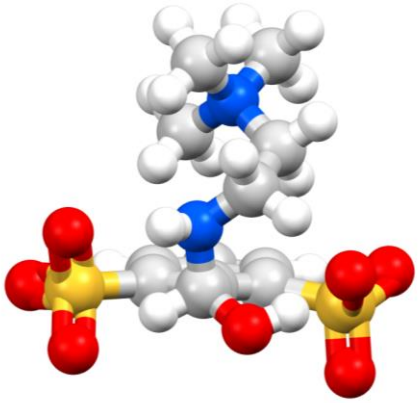

Cartesian coordinates (42 atoms), E (298.15 K) = -1901.34359 Hartree

1	C	-1.0541	0.7336	-0.5418
2	C	0.3590	0.7909	-0.4179
3	C	1.0009	0.8425	-1.1137
4	C	0.2794	0.7168	-1.9336
5	C	-1.7609	0.6110	-1.3594
6	H	0.8150	0.5019	-2.4483
7	H	-2.8359	0.5160	-1.4197
8	S	2.7845	0.2902	-0.9876
9	S	-2.1085	0.4953	0.3394
10	O	3.0373	2.4078	0.4855
11	O	3.5687	1.2098	-1.6423
12	O	2.9196	3.5942	-1.6772
13	O	3.5048	-0.1344	-0.0090
14	O	1.8082	-0.3301	1.7865
15	O	1.7194	-1.8339	-0.1973
16	C	1.0413	-0.3835	0.3388
17	H	0.3711	-0.6359	1.1612
18	O	2.3279	-0.1317	0.8542
19	H	2.4891	0.8231	0.9718
20	N	1.1359	-1.5955	-0.4651
21	H	0.2249	-2.0443	-0.4925
22	C	1.7611	-1.4944	-1.7805
23	H	2.3139	-2.4170	-1.9752
24	H	2.4838	-0.6795	-1.7542
25	C	0.7102	-1.2910	-2.8855
26	H	0.0972	-2.1875	-2.9837
27	H	0.0539	-0.4570	-2.6492
28	C	0.1239	-1.0791	-5.2602
29	H	0.4900	-0.7964	-6.2451
30	H	0.2554	-2.0986	-5.2799
31	H	0.6581	-0.3940	-4.9396
32	C	1.8554	0.3837	-4.3293
33	H	1.0638	1.1017	-4.1265
34	H	2.6337	0.4790	-3.5764
35	H	2.2633	0.5470	-5.3247

36	C	2.3105	-2.0108	-4.6632
37	H	3.1891	-1.8687	-4.0405
38	H	1.9030	-3.0098	-4.5219
39	H	2.5717	-1.8570	-5.7080
40	N	1.2638	-1.0015	-4.2789
41	C	1.0921	2.5914	-2.0797
42	H	1.6380	3.2671	-2.7269

- Lowest energy conformation for the hydrate of **A12**$^{2-}$.

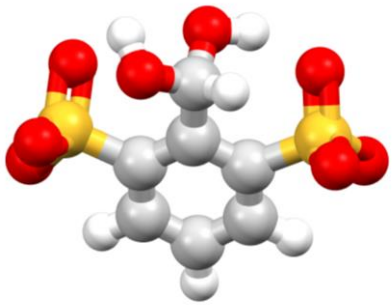

Cartesian coordinates (23 atoms), E (298.15 K) = -1668.96204 Hartree

1	C	1.3406	0.1297	-0.2275
2	C	1.9136	-0.7640	0.6774
3	C	1.1136	-1.6600	1.3711
4	C	-0.2550	-1.6770	1.1347
5	C	-0.8428	-0.7897	0.2292
6	C	-0.0528	0.1629	-0.4504
7	S	-2.6484	-1.1041	-0.0654
8	O	-2.8784	-2.4473	0.5489
9	O	-3.4354	-0.0510	0.6255
10	O	-2.8075	-1.1388	-1.5435
11	S	2.5716	1.1906	-1.1007
12	O	2.0729	1.3869	-2.4989
13	O	3.8201	0.3955	-1.0751
14	O	2.6563	2.4606	-0.3369
15	H	2.9878	-0.7706	0.8032
16	H	1.5586	-2.3702	2.0598
17	H	-0.8843	-2.4074	1.6235
18	C	-0.6022	1.2047	-1.4367
19	H	-0.0096	2.1191	-1.2996
20	O	-0.5034	0.7592	-2.7655
21	H	0.4372	0.8381	-3.0085
22	O	-1.9443	1.5358	-1.1897
23	H	-2.4291	1.2869	-1.9866

- Lowest energy conformation for imine **A12B1**$^{-}$.

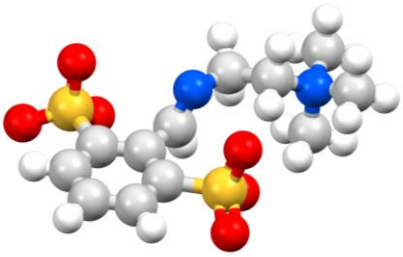

Cartesian coordinates (39 atoms), E (298.15 K) = -1824.89765 Hartree

1	C	-0.262	0.6472	-0.7133
2	C	1.0544	0.5129	-0.2559
3	C	1.9763	1.5245	-0.5702
4	C	1.5972	2.6183	-1.3464
5	C	-0.6412	1.7387	-1.493
6	H	2.3268	3.3874	-1.5635
7	H	-1.6687	1.8135	-1.8243
8	C	1.494	-0.6328	0.5936
9	H	1.3845	-0.4989	1.6731
10	S	3.7084	1.4486	0.0132
11	S	-1.5084	-0.6228	-0.3301
12	O	3.6314	0.9846	1.4281
13	O	4.4042	0.4754	-0.8716
14	O	4.2232	2.834	-0.1214
15	O	-2.8196	0.0325	-0.5753
16	O	-1.281	-0.9674	1.1003
17	O	-1.2334	-1.7496	-1.2599
18	C	2.6576	-2.5891	0.9989
19	H	2.3342	-3.6042	0.7614
20	H	2.3781	-2.3803	2.039
21	C	4.176	-2.4407	0.7782
22	H	4.3904	-1.4282	0.4392
23	H	4.528	-3.1413	0.022
24	C	6.4767	-2.4967	1.5858
25	H	6.6061	-1.4845	1.2089
26	H	7.1184	-2.663	2.4483
27	H	6.7036	-3.22	0.8056
28	C	4.8443	-4.0537	2.5562
29	H	3.808	-4.1738	2.8621
30	H	5.092	-4.7752	1.7804
31	H	5.4985	-4.1849	3.4156
32	C	4.7328	-1.641	3.0728
33	H	4.7157	-0.6562	2.6088
34	H	3.7622	-1.8569	3.5099
35	H	5.5	-1.709	3.8409
36	N	5.04	-2.6678	2.0087
37	C	0.2892	2.7227	-1.8108
38	H	-0.0063	3.5758	-2.4101
39	N	2.0407	-1.6474	0.0716

- Lowest energy conformation for iminium **A12B1**.

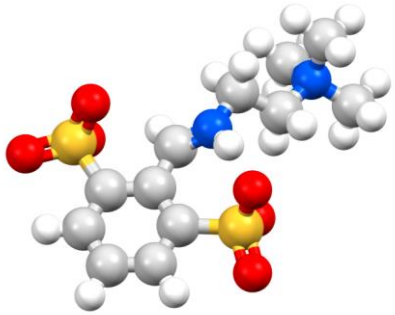

Cartesian coordinates (40 atoms), E (298.15 K) = -1825.344946 Hartree

1	C	-0.2435	0.5747	-1.1964
2	C	0.9825	0.6688	-0.5026
3	C	1.768	1.8324	-0.6823
4	C	1.3328	2.8449	-1.528
5	C	-0.6598	1.5854	-2.0513
6	H	1.9419	3.7319	-1.6366
7	H	-1.5936	1.4689	-2.5843
8	C	1.3252	-0.4255	0.4033
9	H	0.5099	-0.9177	0.9236
10	S	3.3288	2.1223	0.2281
11	S	-1.2843	-0.9191	-1.0302
12	O	2.9745	1.9729	1.6584
13	O	4.2263	1.0113	-0.2516
14	O	3.8051	3.457	-0.1692
15	O	-1.7567	-0.8851	0.38
16	O	-0.3413	-2.0372	-1.2989
17	O	-2.3603	-0.7719	-2.0326
18	C	2.87	-1.7886	1.692
19	H	3.5029	-2.5545	1.2447
20	H	1.9563	-2.2489	2.0635
21	C	3.6147	-0.9897	2.7731
22	H	3.0026	-0.1516	3.1014
23	H	4.5364	-0.583	2.3583
24	C	4.7629	-0.8508	4.9167
25	H	4.1261	-0.0045	5.1636
26	H	5.0328	-1.395	5.8185
27	H	5.6576	-0.5114	4.4001
28	C	4.8849	-2.9517	3.6484
29	H	4.3155	-3.6734	3.069
30	H	5.734	-2.5861	3.0753
31	H	5.2263	-3.416	4.5704
32	C	2.7755	-2.2799	4.7344
33	H	2.131	-1.4322	4.9559
34	H	2.2521	-3.0032	4.1156
35	H	3.0978	-2.7576	5.6564
36	N	3.9994	-1.7839	4.005
37	C	0.1274	2.7209	-2.2148
38	H	-0.1986	3.5149	-2.8755

39	H	3.3176	-0.3355	0.1786
40	N	2.5208	-0.8306	0.6459

6. SambVca details

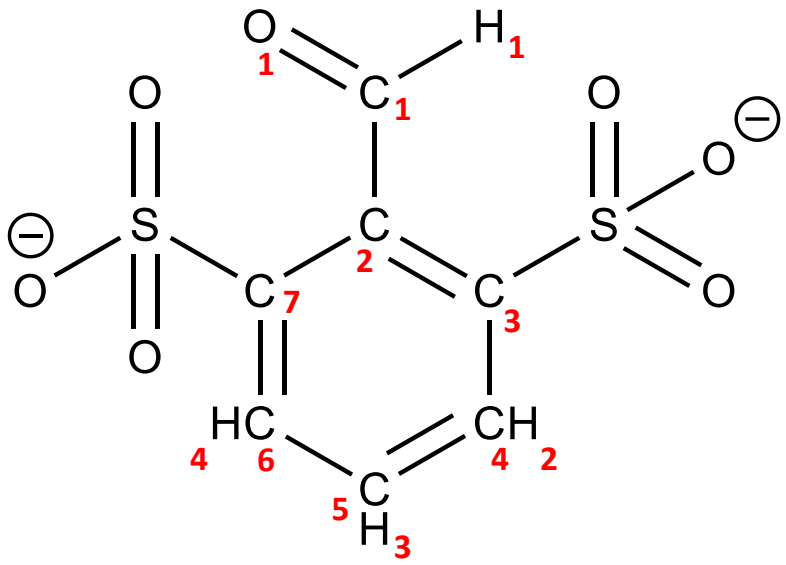

Fig. S36. Selected example (**A12**) for the calculation of the buried volume using SambVca. The centre of the sphere was defined as the C1 atom (carbonyl group), , atom C2 was selected to determine the direction of the z-axis, and atoms C3 and C7were selected to establish the xz-plane. For the buried volume calculation, atoms O1, H1, C1, C2, C3, C4, H2, C5, H3, C6, H4, C7 were deleted so the only crowding effect was that provided by the *ortho*-substituents, in this case the two sulphonate groups.

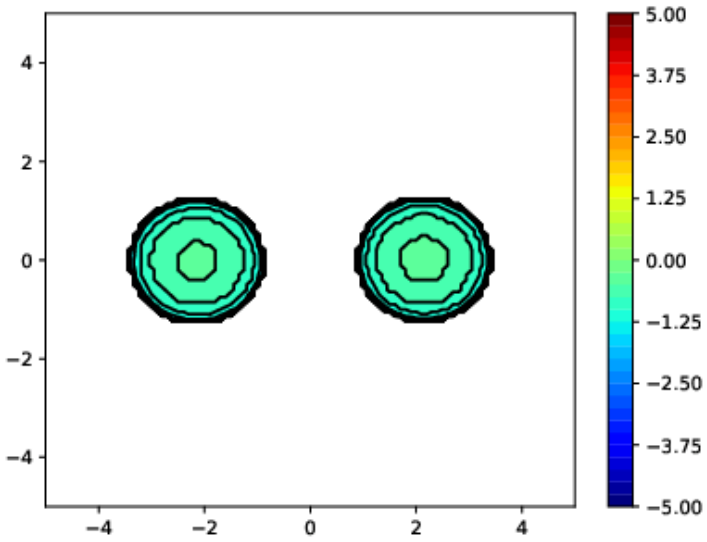

%V Free	%V Buried	% V Tot/V Ex
96.6	3.4	99.9

Quadrant	V f	V b	V t	%V f	%V b
SW	126.3	4.5	130.8	96.6	3.4
NW	126.5	4.3	130.8	96.7	3.3
NE	126.3	4.5	130.8	96.6	3.4
SE	126.5	4.3	130.8	96.7	3.3

Fig. S37. Steric map and related data calculated for **A0** using SambVca.

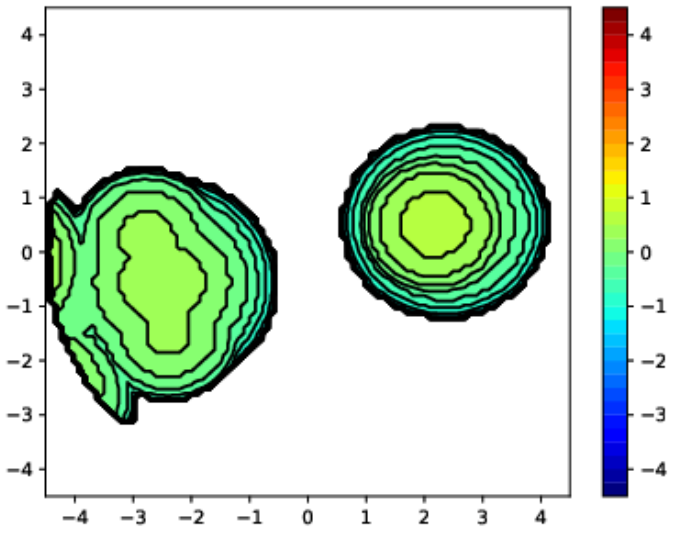

%V Free	%V Buried	% V Tot/V Ex
84.2	15.8	100.0

Quadrant	V f	V b	V t	%V f	%V b
SW	71.2	24.2	95.4	74.6	25.4
NW	84.4	11.1	95.4	88.4	11.6
NE	77.3	18.1	95.4	81.0	19.0
SE	88.5	7.0	95.4	92.7	7.3

Fig. S38. Steric map and related data calculated for **PLP** using SambVca.

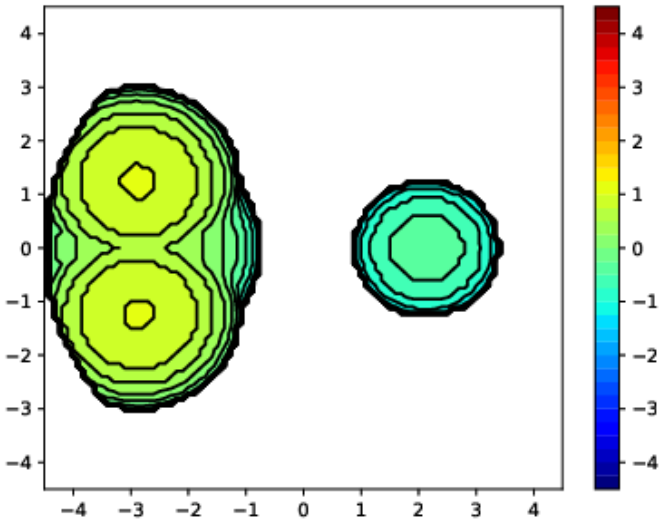

%V Free	%V Buried	% V Tot/V Ex
84.3	15.7	100.0

Quadrant	V f	V b	V t	%V f	%V b
SW	69.9	25.6	95.4	73.2	26.8
NW	69.8	25.6	95.4	73.2	26.8
NE	91.1	4.3	95.4	95.4	4.6
SE	91.0	4.4	95.4	95.4	4.6

Fig. S39. Steric map and related data calculated for **A10** using SambVca.

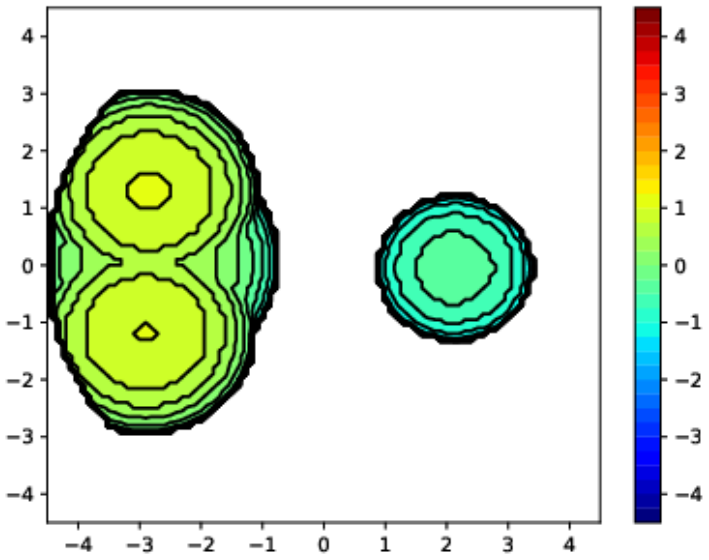

%V Free	%V Buried	% V Tot/V Ex
84.3	15.7	100.0

Quadrant	V f	V b	V t	%V f	%V b
SW	70.5	24.9	95.4	73.9	26.1
NW	69.1	26.3	95.4	72.4	27.6
NE	91.3	4.1	95.4	95.7	4.3
SE	90.8	4.7	95.4	95.1	4.9

Fig. S40. Steric map and related data calculated for **A11** using SambVca.

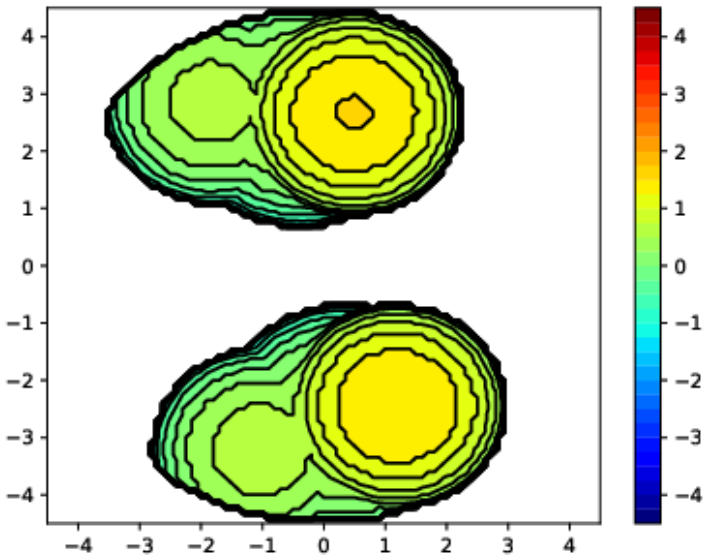

%V Free	%V Buried	% V Tot/V Ex
72.9	27.1	100.0

Quadrant	V f	V b	V t	%V f	%V b
SW	75.1	20.4	95.4	78.7	21.3
NW	66.1	29.3	95.4	69.3	30.7
NE	73.2	22.3	95.4	76.7	23.3
SE	64.1	31.3	95.4	67.2	32.8

Fig. S41. Steric map and related data calculated for **A12** using SambVca.

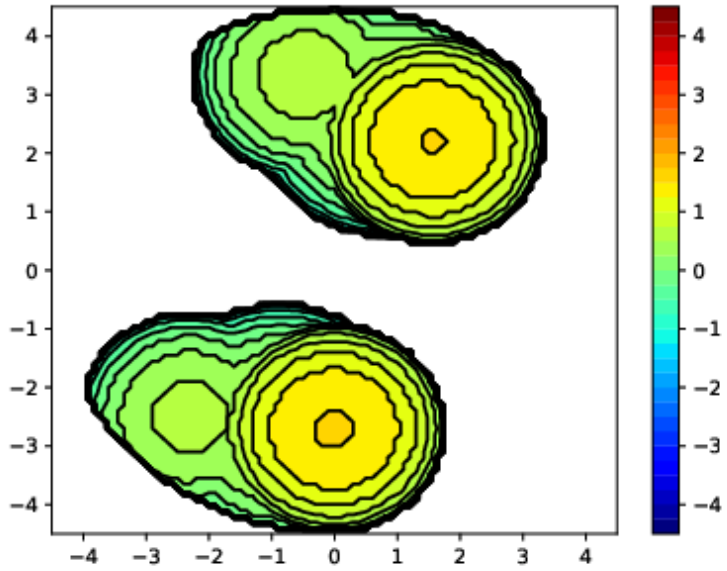

%V Free	%V Buried	% V Tot/V Ex
73.0	27.0	100.0

Quadrant	V f	V b	V t	%V f	%V b
SW	59.5	35.9	95.4	62.4	37.6
NW	80.3	15.1	95.4	84.2	15.8
NE	58.9	36.5	95.4	61.8	38.2
SE	79.9	15.5	95.4	83.8	16.2

Fig. S42. Steric map and related data calculated for **A13** using SambVca.

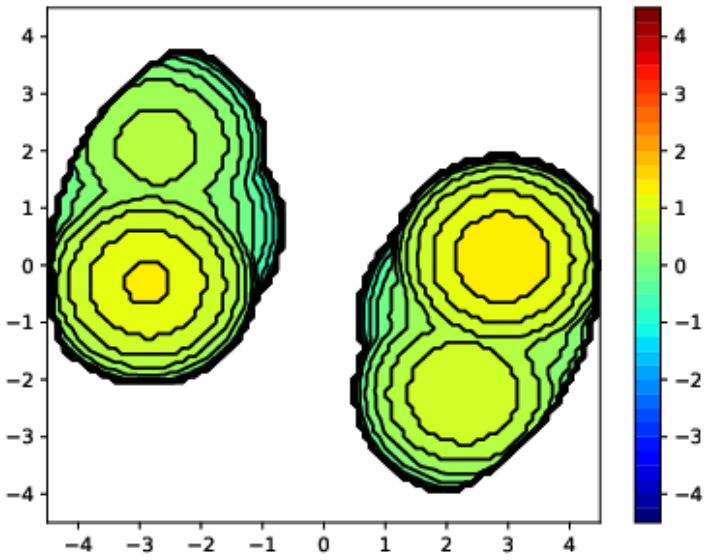

%V Free	%V Buried	% V Tot/V Ex
73.1	26.9	100.0

Quadrant	V f	V b	V t	%V f	%V b
SW	77.3	18.1	95.4	81.0	19.0
NW	63.8	31.6	95.4	66.9	33.1
NE	80.0	15.4	95.4	83.8	16.2
SE	58.0	37.4	95.4	60.8	39.2

Fig. S43. Steric map and related data calculated for **A14** using SambVca.

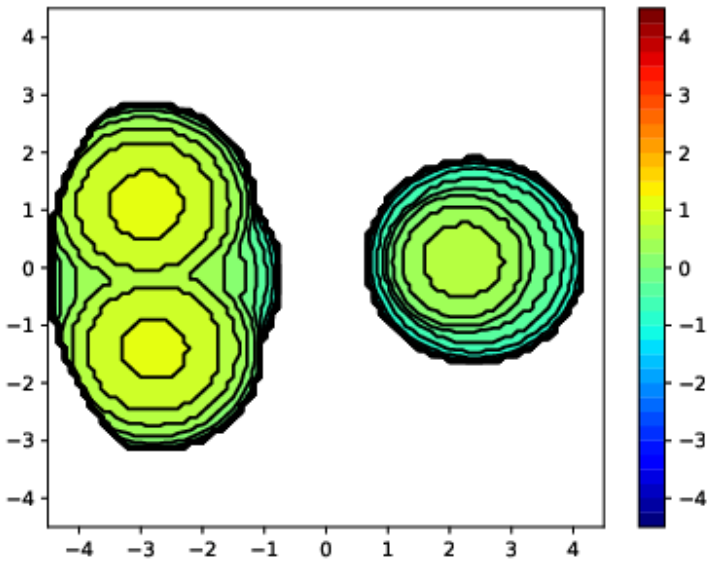

%V Free	%V Buried	% V Tot/V Ex
79.9	**20.1**	100.0

Quadrant	V f	V b	V t	%V f	%V b
SW	67.9	27.5	95.4	**71.2**	28.8
NW	71.2	24.2	95.4	**74.6**	25.4
NE	81.5	13.9	95.4	**85.4**	14.6
SE	84.2	11.3	95.4	**88.2**	11.8

Fig. S44. Steric map and related data calculated for **A15** using SambVca.

7. References

[1] M. J. A Frisch, G. W. Trucks, H. B. Schlegel, G. E. Scuseria, M. A. Robb, J. R. Cheeseman, G. Scalmani, V. Barone, B. Mennucci, G. A. Petersson, *et al.* Gaussian 09, Revision B.01 (Gaussian, Inc), 2010.

[2] S. Miertus and J. Tomasi, *Chem. Phys.,* 1982, **65**, 239–241.

[3] S. Grimme, J. Antony, S. Ehrlich and H. Krieg, *J. Chem. Phys.,* 2010, **132**, 154104.

[4] L. Falivene, Z. Cao, A. Petta, L. Serra, A. Poater, R. Oliva, V. Scarano and L. Cavallo, *Nat. Chem.,* 2019, **11**, 872-879.

[5] L. Falivene, R. Credendino, A. Poater, L. Serra, A. Petta, R. Oliva, V. Scarano and L. Cavallo, *Organometallics,* 2016, **35**, 2286-2293.

[6] GNU v.3 (Free Sofware Foundation, 2007).

[7] T. Fiala, J. Wang, M. Dunn, P. Šebej, S. J. Choi, E. C. Nwadibia, E. Fialova, D. M. Martinez, C. E. Cheetham, K. J. Fogle, M. J. Palladino, Z. Freyberg, D. Sulzer and D. Sames, *J. Am. Chem. Soc.,* 2020, **142**, 9285−9301.